Backtracked and paused transcription initiation intermediate of *Escherichia coli* RNA polymerase

Eitan Lerner[a,1], SangYoon Chung[a,1], Benjamin L. Allen[b,1], Shuang Wang[c,1], Jookyung Lee[d], Shijia W. Lu[a], Logan W. Grimaud[a], Antonino Ingargiola[a], Xavier Michalet[a], Yazan Alhadid[a], Sergei Borukhov[d], Terence R. Strick[c,e,f,2], Dylan J. Taatjes[b,2], and Shimon Weiss[a,g,h,2]

[a]Department of Chemistry & Biochemistry, University of California, Los Angeles, CA 90095; [b]Department of Chemistry & Biochemistry, University of Colorado, Boulder, CO 80309; [c]Institut Jacques Monod, Centre National de la Recherche Scientifique (CNRS), UMR7592, University Paris Diderot, Sorbonne Paris Cité, F-75205 Paris, France; [d]Rowan University School of Osteopathic Medicine, Stratford, NJ 08084; [e]Institut de Biologie de l'Ecole Normale Supérieure, Institut de Biologie de l'Ecole Normale Superieure (IBENS), CNRS, Inserm, Ecole Normale Supérieure, Paris Sciences et Lettres (PSL) Research University, F-75005 Paris, France; [f]Programme Equipe Labellisées, Ligue Contre le Cancer, 75013 Paris, France; [g]Molecular Biology Institute, University of California, Los Angeles, CA 90095; and [h]Department of Physiology, University of California, Los Angeles, CA 90095

Edited by Steven M. Block, Stanford University, Stanford, CA, and approved September 13, 2016 (received for review March 30, 2016)

Initiation is a highly regulated, rate-limiting step in transcription. We used a series of approaches to examine the kinetics of RNA polymerase (RNAP) transcription initiation in greater detail. Quenched kinetics assays, in combination with gel-based assays, showed that RNAP exit kinetics from complexes stalled at later stages of initiation (e.g., from a 7-base transcript) were markedly slower than from earlier stages (e.g., from a 2- or 4-base transcript). In addition, the RNAP–GreA endonuclease accelerated transcription kinetics from otherwise delayed initiation states. Further examination with magnetic tweezers transcription experiments showed that RNAP adopted a long-lived backtracked state during initiation and that the paused–backtracked initiation intermediate was populated abundantly at physiologically relevant nucleoside triphosphate (NTP) concentrations. The paused intermediate population was further increased when the NTP concentration was decreased and/or when an imbalance in NTP concentration was introduced (situations that mimic stress). Our results confirm the existence of a previously hypothesized paused and backtracked RNAP initiation intermediate and suggest it is biologically relevant; furthermore, such intermediates could be exploited for therapeutic purposes and may reflect a conserved state among paused, initiating eukaryotic RNA polymerase II enzymes.

transcription | pausing | backtracking | RNAP | RNA polymerase

Transcription in *Escherichia coli* comprises three stages: initiation, elongation and termination. Initiation, which is typically the rate-limiting and the most regulated stage of transcription, is by itself a complex, multistep process consisting of the following successive steps (1, 2): (*i*) association of RNA polymerase (RNAP) core enzyme (subunit composition $\alpha 2\beta\beta'\omega$) with the promoter specificity factor σ (such as σ70 for transcription of housekeeping genes) to form RNAP holoenzyme; (*ii*) binding of holoenzyme to the −10 and −35 DNA elements in the promoter recognition sequence (PRS) upstream to the transcription start site (TSS) to form closed promoter complex (RPc); (*iii*) isomerization of RPc through multiple intermediates into an open promoter complex (RPo), in which a ∼12-bp DNA stretch (bases at registers −10 to +2) is melted to form a transcription bubble, the template DNA strand is inserted into RNAP major cleft positioning the base at register +1 of TSS at the active site, the nontemplate strand is tightly bound by σ70 and the downstream DNA duplex (bases +3 up to +20) is loaded into RNAP β′ DNA-binding clamp; (*iv*) an abortive initiation step (AI), where binding of nucleoside triphosphate (NTPs) and the start of RNA synthesis leads to formation of an initial transcribing complex (RP_{ITC}) followed by RNAP cycling through multiple polymerization trials via a DNA scrunching mechanism (3, 4), release of short "abortive transcripts" and repositioning itself in RP_O for a new synthesis trial (5–7); and finally, (*v*) RNAP promoter escape, when enough strain is built in the enzyme, the σ70 undergoes structural transition to relieve blockage of the RNA exit channel in RNAP and loses its grip on the PRS, nascent RNA enters the RNA exit channel and transcription enters the elongation stage.

In AI, the interactions between σ70 and the PRS limit the lengths of abortive transcripts. The stronger these interactions are, the longer the time RNAP will spend cycling in AI (8) and the longer the lengths of abortive transcripts will be (9). For these reasons, after establishing tight promoter interactions, transcription initiation is rather slow. Transcription elongation, on the other hand, is a very efficient and fast process (10–13). However, in elongation, RNAP may encounter specific sequences that cause transcriptional pausing, sometimes accompanied by backtracking of the RNA chain pushing its 3′ end into the RNAP secondary channel (14), the site of NTPs entry (15). Pausing and pause release in elongation constitute additional steps (discussed below).

Whereas the basic biochemical steps of RNA polymerization (including NTP entrance and insertion, phosphodiester bond formation, pyrophosphate removal and RNAP translocation) are the same both in initiation and in elongation, their overall rates are far slower in initiation due to the structural differences

Significance

Transcription initiation by RNA polymerase (RNAP) is a highly regulated rate-limiting step in many genes and involves numerous intermediate states that remain incompletely understood. Here, we report the characterization of a previously hypothesized slow initiation pathway involving RNAP backtracking and pausing. This backtracked and paused state is observed when all nucleoside triphosphates (NTPs) are present at physiologically relevant concentrations, but becomes more prevalent with unbalanced NTP levels, which may occur in vivo under conditions of metabolic stress. Pausing and backtracking in initiation may play an important role in regulating RNAP transcription. Moreover, similar RNA backtracked states may contribute to promoter-proximal pausing among eukaryotic RNA polymerase II enzymes.

Author contributions: E.L., S.C., B.L.A., S. Wang, and S. Weiss designed research; E.L., S.C., B.L.A., S. Wang, S.W.L., L.W.G., Y.A., T.R.S., and D.J.T. performed research; S.C., J.L., A.I., X.M., and S.B. contributed new reagents/analytic tools; E.L., S.C., B.L.A., S. Wang, S.B., T.R.S., D.J.T., and S. Weiss analyzed data; E.L., S.C., B.L.A., S. Wang, S.B., T.R.S., D.J.T., and S. Weiss wrote the paper; E.L., S.C., T.R.S., D.J.T., and S. Weiss designed this study; E.L. and S.C. developed and designed the quenched-kinetics experiments; E.L., S.C., S.W.L., L.W.G., and Y.A. performed the quenched-kinetics measurements, in consultation with A.I. and X.M; B.L.A. designed and performed gel-based experiments; S. Wang and T.R.S. designed, performed, and analyzed magnetic tweezers experiments; and J.L. and S.B. prepared GreA protein.

The authors declare no conflict of interest.

This article is a PNAS Direct Submission.

[1]E.L., S.C., B.L.A., and S. Wang contributed equally to this work.

[2]To whom correspondence may be addressed. Email: sweiss@chem.ucla.edu, strick@biologie.ens.fr, or taatjes@colorado.edu.

This article contains supporting information online at www.pnas.org/lookup/suppl/doi:10.1073/pnas.1605038113/-/DCSupplemental.

between these states (16–18). In particular, the strong σ70–PRS interactions (absent in elongation) (19–21) and the interactions (steric and electrostatic) of the acidic tip of the σ70 region 3.2 (σR3.2, which blocks the RNA exit channel) and the 5′ end of the nascent transcript (22–25) contribute most to the slow rate of initiation. Nascent RNAs of up to 9 nt in length are stabilized by hybridization to the melted template DNA in the RNA:DNA hybrid (18, 26–28). Although RNAP can accommodate an RNA of up to 14 nt long (i.e., 9 nt in RNA:DNA hybrid + 5 nt in RNA exit channel) (29), the transition into elongation, whereby the RNA exit channel blockage by σR3.2 is relieved, begins when RNA reaches the length of 11 nt (16, 30–32). After removal of the exit channel blockage, RNAP undergoes a global conformational change, σ70 loses its grip on the PRS and RNAP processively and rapidly elongates until it reaches the termination signal (23).

In what ways can RNAP overcome the barrier between initiation and elongation? Previous experimental data suggested that in AI, RNAP scrunches downstream DNA into its active site (3, 4). Because σ70 holds the −10 and −35 DNA elements tightly, the dsDNA upstream to the transcription bubble stays as a duplex, whereas the 10 DNA bases in the noncoding part of the transcription bubble (bases −10 to −1 in both strands) become compressed. This results in a strain buildup into what is known as the "stressed intermediate" complex (5, 33). Additionally, the longer the initially transcribed nascent RNA is, the closer its negatively charged 5′ end will be to the acidic tip of σR3.2 (19, 24). Simultaneously, a longer nascent transcript makes more stable RNA:DNA hybrid, which, in turn, helps counteract strain from the compressed DNA bubble and electrostatic repulsion from the acidic tip of σR3.2. In AI, transcripts are held in RNAP until reaching a certain length, above which the strain is relieved either through RNA backtranslocation and its abortive release through the secondary channel (14, 34–36) or by pushing σR3.2 and unblocking the RNA exit channel (22–25).

The electrostatic repulsion between the acidic tip of σR3.2 and the negatively charged 5′ end of the nascent transcript should decrease with each backtranslocation step (i.e., the distance between the negatively-charged groups increases). Nascent transcripts >4 nt in length could be stabilized in a backtracked state resulting in initiation pausing without immediate abortive release. Similar situations in elongation stabilize the nascent transcript in the pretranslocated state (37–41), eventually causing the nascent RNA 3′ end to disengage from the active site, backtrack into the secondary channel and pause transcription. The backtracked RNA can be cleaved either by the intrinsic endonucleolytic activity of RNAP (very inefficient at physiological pH) or by the action of extrinsic transcript cleavage factors GreA and GreB (TFIIS in eukaryotic RNA polymerase II system (42)). This cleavage leads to realignment of the newly formed RNA 3′-terminus with the active site and reactivation of transcription (pause release) (43–45). Due to these parallels, we wanted to examine if backtracking and pausing occur in transcription initiation by RNAP as well.

Previously it has been shown that stalling of transcription initiation occurs in strong promoters (8, 46). In addition, it has been shown that GreA and GreB induce RNA cleavages in AI, reduce abortive cycling and stimulate RNAP transition to elongation in vitro and in vivo at certain promoters (5, 25, 47–55). Linking these

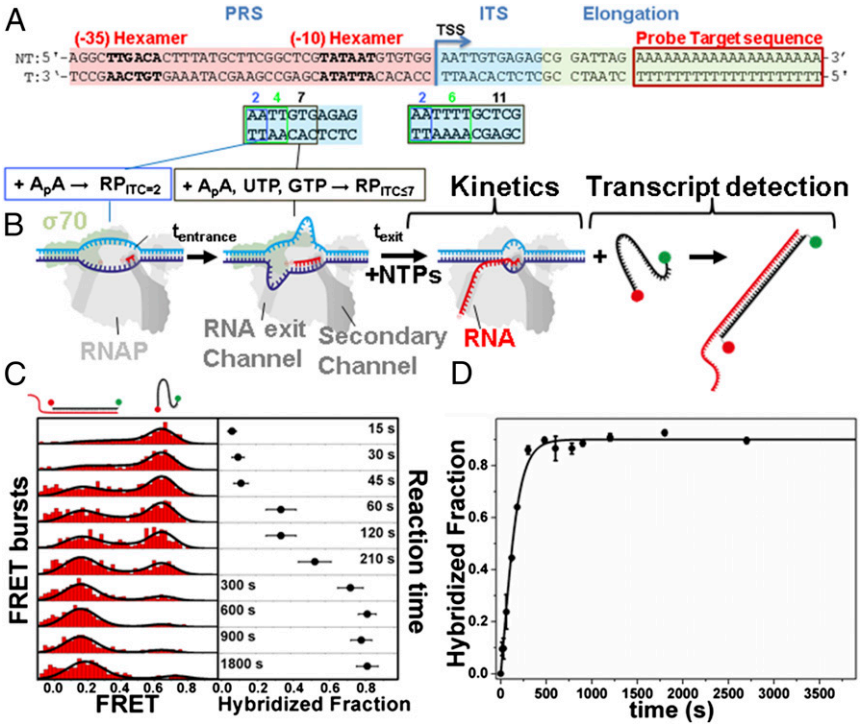

Fig. 1. Single-round transcription quenched kinetics assay. (*A*) Representative promoter sequence used here (lacCONS promoter) to show how by changing the initially transcribed sequence (ITS; cyan), different NTP-starved states can be generated ($RP_{ITC=2}$, $RP_{ITC\leq4,6,7}$, $RD_{E=11}$). Other regions of the promoter include the promoter recognition sequence (PRS; pink) and the elongation sequence (yellow), including a probe target complementary sequence (red). All promoters measured are described in Fig. S1. (*B*) Schematic of RNAP runoff transcription starting from a particular NTP-starved state (incubation with a partial set of NTPs for $t_{entrance}$). Upon supplementing all NTPs, transcription kinetics start and transcripts are quantified via hybridization to a ssDNA FRET probe for different incubation times (t_{exit}). (*C*) Example of quenched kinetics data generated from quantification of runoff transcripts. The example follows one repetition of the kinetics exiting from $RP_{ITC=2}$. (*D*) As an example for kinetic curve extraction, average runoff kinetics from various $RP_{ITC=2}$ are shown. The data points are averages of three repeats and the error bars are the SDs about these averages. The data are represented as points and the solid line represents the best-fit result to the model described in *Methods*. The best-fit values of the model parameters are shown in Table S1.

biochemical studies to the aforementioned endonucleolytic activity that the GreA–RNAP complex has in elongation, it was hypothesized that RNAP backtracking may occur in initiation and that GreA factors, as in elongation, act upon the nascent RNA bases that enter into the secondary channel of RNAP through backtracking. To directly address this question and to study the mechanism of transcription initiation in greater detail, we developed a solution-based, single-round quenched kinetics transcription assay that measures the kinetics of runoff transcript production. This assay was initially used to assess the kinetics of exit out of NTP-starved RP_{ITC} states, using an *E. coli* transcription system reconstituted from native RNAP core enzyme and σ70. Such NTP-starvation experiments provided us with reliable means to interrogate RNAP transcription from specific initiation states and offered mechanistic insights that were further validated in the follow-up experiments with minimal or no starvation. In addition to quenched kinetics assays of runoff RNA, we performed gel-based in vitro transcription assays that focused on kinetics of abortive products. Finally, we carried out single-molecule magnetic tweezers experiments to monitor changes in transcription bubble size during transcription initiation by RNAP. Altogether, we report here the detection and direct observation of RNAP in a backtracked, paused state during early stages of transcription initiation. Although previously hypothesized, our results establish paused, backtracked RNAP as a bona fide initiation intermediate. This observation could have potential applications for molecular therapeutics and mechanistic implications for mammalian RNA polymerase II enzymes.

Results and Discussion

Single-Round Transcription Quenched Kinetics Assay. We developed a single-round quenched kinetics assay (Fig. 1) to probe the kinetics of transcription by directly counting the number of transcripts produced over time. Using this assay, we initially examined the kinetics of *E. coli* RNAP transcription from distinct RP_{ITC} states generated via NTP starvation (Fig. 1 *A* and *B*). The assay was based on quantification of single runoff transcripts by hybridization with a doubly labeled ssDNA probe (Fig. 1*B*). The number of hybridized probes (and hence the number of transcripts) was accurately determined using microsecond alternating-laser excitation (μsALEX)-based fluorescence-aided molecule sorting (ALEX-FAMS) (56, 57) (Fig. 1*C*). ALEX-FAMS is a method based on single-molecule Förster resonance energy transfer (smFRET) (58). A significant advantage of smFRET and ALEX-FAMS is the ability to identify distinct populations in a model-free manner, simply by counting single-molecule events of one sort (with a given FRET efficiency population) and comparing their number to single-molecule events of another sort (representing a distinct FRET efficiency population) (56, 57, 59, 60) (Fig. 1*C*). Hence, FAMS is a suitable method for the quantification of runoff transcripts at picomolar probe concentrations.

Our experimental design circumvented potential drawbacks of the quenched kinetics assay. Because we used low concentrations of RNAP and promoter DNA, the probability for RNAP reassembly/reinitiation was low, whereas single-round transcription reaction conditions were achieved kinetically and thermodynamically (61, 62) (details in *Supporting Information*, *Rationale of the Single-Round Character of the Quenched Kinetics Transcription Assay*). Furthermore, we designed the DNA template so that the probe hybridization sequence would anneal at the end of the fully elongated RNA (Fig. 1*A*); in this way, probe hybridization would not interfere with transcription initiation but instead report on successful promoter escape. Also, because transcription initiation in many genes is much slower than elongation (i.e., initiation is typically rate limiting) (63), the synthesis of relatively short, yet full-length RNA products (39-base and 41-base transcripts for the promoters studied here) reflected the rate of transcription initiation.

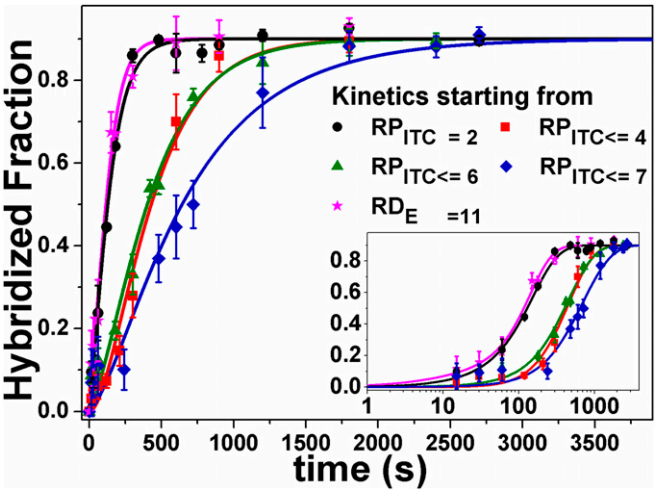

Fig. 2. Quenched kinetics transcription results identify an initiation-related stalled state. Shown are runoff kinetics from various NTP-starved states. Kinetics starting from late initiation states (e.g., $RP_{ITC\leq7}$, blue) are slower than from an earlier initiation state (e.g., $RP_{ITC=2}$, black). The data are represented as points and solid lines represent best-fit results to the model described in *Methods*. The best-fit values of the model parameters are shown in Table S1.

The ssDNA probe was doubly labeled with a FRET pair. When free in solution, the probe yields a single FRET population with a peak FRET efficiency of E ~ 0.75 (Fig. 1*C*). Hybridization of the ssDNA FRET probe with the elongation part of the runoff transcript yields a FRET efficiency population with a lower peak value of E ~ 0.3, due to the probe being stretched via hybridization to the 20A target sequence segment of the runoff transcript (Fig. 1 *A* and *C*). Correct assessment of transcription initiation rates by the quenched kinetics assay requires (*i*) formation of a stable initial state, (*ii*) addition of NTPs at t = 0, (*iii*) efficient and rapid quenching of the reaction at selected times, (*iv*) full hybridization of the ssDNA FRET probe to transcripts and (*v*) prevention of RNA degradation. As outlined below, our experiments were conducted under conditions that satisfied each of these requirements.

i) The formation of a stable initial transcribing state was achieved by using partial sets of NTPs that limited transcript polymerization to a given maximal length, which was dependent on the initially transcribed sequence (ITS) of the promoter DNA. We used the ITS of either the lacCONS (64, 65) (Fig. 1*A* and Fig. S1) or T5N25 (4) (Fig. S1) promoters, which allowed production of abortive transcripts of varying maximal lengths upon addition of different partial NTP sets (Fig. S1). Stable open complexes were formed by adding an initiating dinucleotide to achieve $RP_{ITC=2}$ (control measurements in Figs. S2 and S3; detailed discussion in *Supporting Information*, *Initiating Dinucleotide With/Without a 5′-Triphosphate Group*). To stabilize an RP_{ITC} state ($RP_{ITC\leq i}$, i ϵ [4,6,7]) or an RNAP–DNA elongation complex state ($RD_{E=11}$), $RP_{ITC=2}$ was incubated for a given time, $t_{entrance}$, in the presence of a partial set of NTPs (Fig. 1*B*).

ii) In the absence of specific NTPs, NTP-starved RP_{ITC} or RD_E states should not produce runoff transcripts. The stability of NTP-starved RP_{ITC} or RD_E states was verified by negative control experiments, in which ssDNA FRET probe ALEX-FAMS measurements were performed with a limited set of NTPs, whereby hybridization of the FRET probe was not observed, and hence no runoff transcript was produced. Only after all four NTPs were added were runoff transcripts detected. Therefore, for the purposes of the assays described herein, the time at which all NTPs were added was set as t = 0.

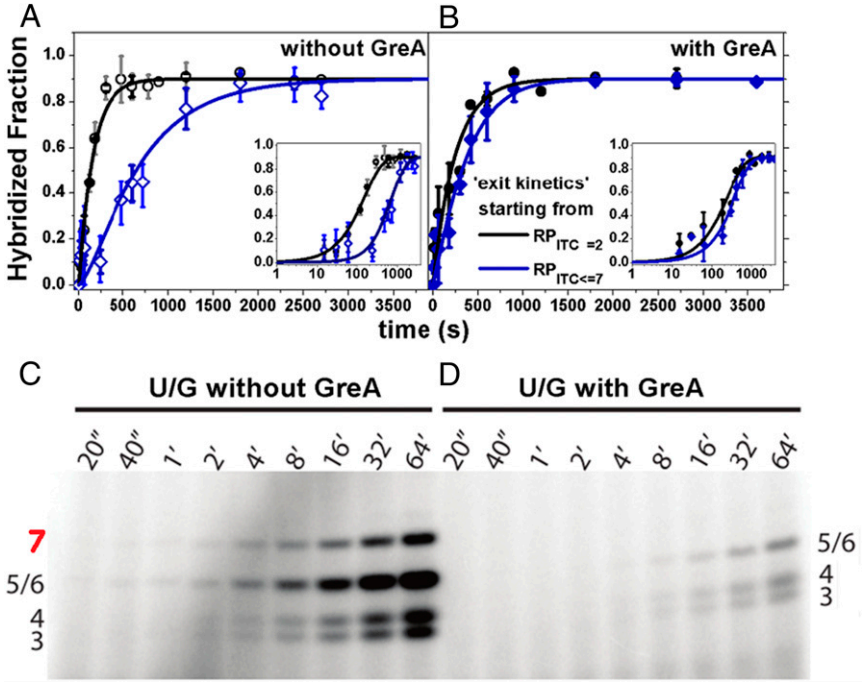

Fig. 3. GreA suppresses the kinetic delay in transcription initiation. (*A*) Runoff transcription kinetics are slower when starting from $RP_{ITC\leq7}$ (blue) than from $RP_{ITC=2}$ (black) (Fig. 2). (*B*) With 1 μM GreA, the delay in transcription initiation is reduced. The data are represented as points and solid lines represent best-fit results to the model described in *Methods*. The best-fit values of the model parameters are shown in Table S1. (*C* and *D*) Gel-based abortive initiation kinetics: Without GreA, NTP-starved $RP_{ITC\leq7}$ produced abortive transcripts up to 7 bases long, whereas the 7-base product was not produced with 1 μM GreA, suggesting 2 bases of 3′-backtracked RNA were cleaved by RNAP in a GreA-catalyzed reaction during initiation. Band assignment is provided in Fig. S8*A* and the accompanying legend.

iii) The kinetics of runoff transcript production, starting from an NTP-starved state, were measured using a constant $t_{entrance}$ = 40 min, followed by a varying incubation time with all four NTPs (t_{exit}), followed by efficient quenching of the transcription reaction. $t_{entrance}$ = 40 min was selected to be in the plateau of the measured ∼7-min entrance kinetics (Fig. S4). Guanidinium hydrochloride (GndHCl; 0.5 M) served both as a reaction quencher (Fig. S5) and as an enhancer of hybridization of the ssDNA FRET probe to the runoff transcript (Fig. S6).

iv) After quenching the transcription reaction, the 20-base ssDNA FRET probe was added. The hybridization of the ssDNA FRET probe to the elongation segment of the runoff transcript was probed by ALEX-FAMS (Fig. 1*C*). The number of runoff transcripts per time point was calculated from the results of a global fit to the ALEX-FAMS–derived FRET histograms to a two-Gaussian model (Fig. 1*C* and *Supporting Information*, *μsALEX-smFRET Analysis for the Quantification of Transcription Kinetics*). Then the fraction of events in the low-FRET subpopulation, "hybridized fraction" (the number of runoff transcripts produced, relative to known amount of ssDNA FRET probe) is plotted as a function of t_{exit} (Fig. 1*C*). Repeats of the same measurement are performed to produce reliable averaged kinetic curves (as in Fig. S7) that can be later used for curve fitting (Fig. 1*D*).

v) Throughout the experiments, an RNase inhibitor was added to the reaction mixture to prevent degradation of RNA products.

Slower Transcription Initiation Kinetics from Select NTP-Starved States. Because promoter escape is the rate-limiting step in initiation, we anticipated that RNAP transcription kinetics starting from different RP_{ITC} states ("exit kinetics") would be similar. However, we found that exit kinetics from the $RP_{ITC\leq4}$, $RP_{ITC\leq6}$, or $RP_{ITC\leq7}$ states were slower than from $RP_{ITC=2}$ state (Fig. 2). In fact, whereas exit kinetics from $RP_{ITC=2}$ were similar to those of RNAP already in the elongation state ($RD_{E=11}$), the exit kinetics from $RP_{ITC\leq7}$ were at least 3.5 times slower (Table S1). These results suggested the existence of a previously hypothesized paused state in RNAP transcription initiation ($RP_{ITC\leq i}$*; see Fig. 5). Importantly, this state was transient and overall RNAP activity remained unchanged, given that all "delayed" RNAP complexes ($RP_{ITC\leq4}$, $RP_{ITC\leq6}$, or $RP_{ITC\leq7}$) eventually transitioned to elongation (Fig. 2).

Delayed Initiation Kinetics Are Associated with Backtracking. It is well established that elongating RNAP can backtrack and pause (44, 45). In such circumstances, the nascent RNA 3′ end backtranslocates into the secondary channel, where it can undergo endonucleolytic cleavage by the GreA–RNAP complex (25, 44, 48, 66). To test whether delayed exit kinetics for $RP_{ITC\leq7}$ were associated with backtracking during initiation, we assessed the effect of GreA, using our single-round quenched kinetics assay. As shown in Fig. 3 *A* and *B*, the addition of GreA at physiologically relevant concentration of 1 μM accelerated the exit kinetics from $RP_{ITC\leq7}$ relative to the exit kinetics from $RP_{ITC=2}$ (∼50% recovery from the $RP_{ITC\leq7}$* stalled state; *Methods* and Table S1). These results were consistent with GreA-dependent release of RNAP from a backtracked and paused state in elongation (44, 45, 47).

To further test the effect of GreA during RNAP transcription initiation, we performed in vitro transcription assays in which ^{32}P-labeled abortive transcripts were quantified following polyacrylamide gel electrophoresis (PAGE). This enabled identification of various abortive transcripts (band assignment in Fig. S8*A* and accompanying legend) and thus provided a means to determine whether GreA catalyzed the cleavage of short transcripts during transcription initiation. As shown in Fig. 3 *C* and *D*, the

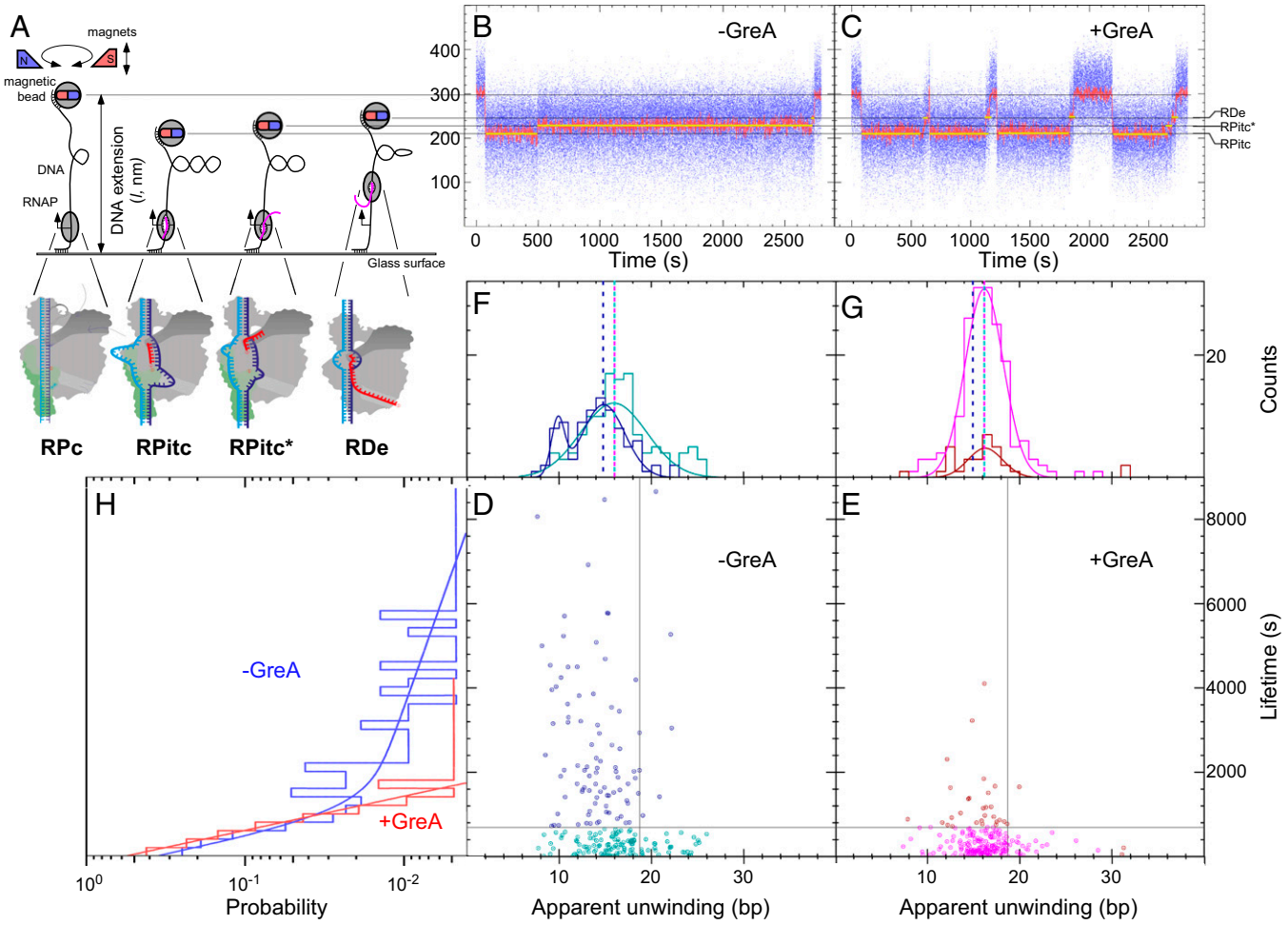

Fig. 4. Backtracking in initiation correlates with RNAP pausing in the presence of equimolar NTPs. (*A*) Schematics of the magnetic tweezer transcription assay (*Methods*). (*B* and *C*) Representative bead extension trajectories shown for single-molecule transcription experiments without (*B*) or with (*C*) 1 μM GreA. Unwinding levels (gray lines) are shown, indicating different bubble sizes imposed by different RNAP states (below). Yellow lines highlight typical lifetimes in each state. (*D–H*) Unwinding levels and RP_{ITC} and RP_{ITC}* lifetimes of individual initiation events (i.e., averaging over all RP_{ITC} and RP_{ITC}* states seen from initiation to promoter escape) are summarized into unwinding–lifetime scatter plots without (*D*) or with (*E*) 1 μM GreA; their 1D projections are shown in *F–H*. Quadrant structure is built as discussed in *Methods*, *Illustrations*. Lifetime data in the absence or presence of GreA were first fitted to single or double exponentials based on goodness-of-fit. Then, the 2D data were temporally separated into events shorter than (cyan, absence of GreA; magenta, presence of GreA) or longer than (dark blue, absence of GreA; dark red, presence of GreA) the fast timescale for promoter escape (~300 s) plus 1 SD. Similarly, the 2D data were spatially separated into events with apparent unwinding amplitude smaller or larger than the mean unwinding observed during short-duration escape events plus 1 SD. Apparent unwinding data associated with short- or long-escape timescales were then fitted to single- or double-Gaussian distributions based on goodness-of-fit and according to the color code described above. Dotted vertical lines are visual guides to the maximum of the respective Gaussian distributions. Twenty to fifty DNA templates, carrying the lacCONS promoter sequence, were used for each condition, with 5–10 transcription pulses per template.

production of the 7-base abortive RNA transcript was significantly suppressed in the presence of GreA. Because GreA stimulates cleavage only of "backtracked" RNA (i.e., when the RNA 3′ end is inserted into the secondary channel), these data, combined with our single-round kinetics data, confirmed that RNAP backtracks during transcription initiation. Because GreA predominantly induces cleavage of 2–3 bases from the RNA 3′-terminus (44, 45, 50–52), the lack of the 7-base abortive transcript is most likely due to GreA-induced shortening (compare Fig. 3 *C* and *D*) to a 5-mer, suggesting that RNAP in NTP-starved $RP_{ITC\leq 7}$ backtracks by 1 base.

RNAP Backtracking and Pausing in the Presence of All NTPs. The data summarized in Figs. 2 and 3 studied pausing and backtracking in RNAP transcription initiation under conditions in which one or more NTPs were absent. Whereas the complete absence of select NTPs is highly unlikely in vivo, changes in pools of NTP levels may occur in bacteria in several conditions (e.g., metabolic stress, stages in cell growth; discussions in refs. 67–69). Accordingly, we examined RNAP transcription with the quenched kinetics assay with all NTPs present but under NTP concentration imbalance (UTP and GTP >> ATP and CTP at the lacCONS promoter; UTP and ATP >> CTP and GTP at the T5N25 promoter). According to the DNA sequences of these promoters (Fig. S1), these conditions were expected to temporarily populate delayed RP_{ITC} states ($RP_{ITC\leq 7}$ in lacCONS and $RP_{ITC\leq 8}$ in T5N25, respectively). Consistent with the results described above, we observed a delay in exit kinetics from the $RP_{ITC=2}$ state under conditions of NTP imbalance (Fig. S9, orange) compared with equimolar conditions (Fig. S9, black) at each of the two different tested promoter templates. In addition, the observed delay was smaller in magnitude than the delay achieved upon exit from an NTP-starved RP_{ITC} state (Fig. S9, blue). This result implies the kinetic delay inversely correlates with the abundance of the NTPs required for promoter clearance.

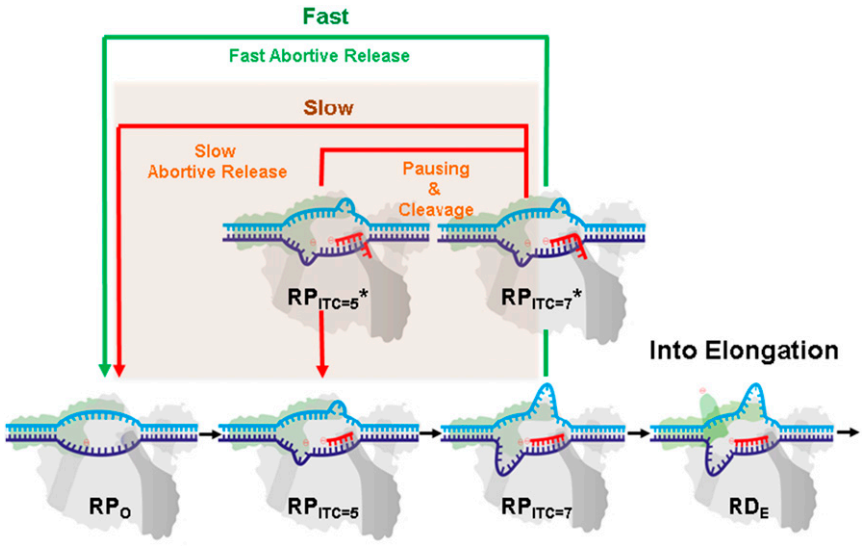

Fig. 5. A modified transcription initiation model. RNAP transcription initiation branches to (*i*) promoter clearance and transitions into elongation (black arrows) or into (*ii*) release of abortive transcripts (green and red arrows). After initial backtracking steps (e.g., from $RP_{ITC=7}$ to $RP_{ITC=7*}$), the complex can continue with either (*iii*) fast abortive transcript release (classic model, green arrow) or (*iv*) transition into a paused and backtracked state. Exit from the paused–backtracked state can occur either by successive slow backtracking steps (red arrow) or through intrinsic cleavage of RNA bases that are in the secondary channel, which prepares RNAP in, e.g., the $RP_{ITC=5}$ state. Upon cleavage, the complex can release the abortive transcript or reestablish RNA polymerization (e.g., from the $RP_{ITC=5}$ state).

The single-round quenched transcription kinetics assay and transcription assays with ^{32}P-labeled UTP are ensemble experiments and hence cannot reliably detect infrequent or transient events. Under conditions of NTP starvation, abortive transcripts are identifiable by the gel-based assay (Fig. 3*B*). However, in the presence of all NTPs we did not obtain radiolabeled bands with sufficient intensity for the quantification of abortive transcripts, due to a limited number of abortive transcripts produced under single-round transcription conditions (Fig. S8*B*). The single-round transcription kinetics starting from $RP_{ITC=2}$ may already be influenced by pausing and backtracking; however, in the quenched kinetics assay $RP_{ITC=2}$ serves as a reference point.

To detect the full initiation behavior on the lacCONS promoter in the presence of equimolar NTPs (100 μM each) with high sensitivity, we implemented magnetic tweezers experiments with positively supercoiled promoter templates (Fig. 4*A*). This assay allowed us to track individual RNAP complexes over time and simultaneously detect and identify distinct RP_{ITC} states, based upon well-established changes in DNA extension (4). In the absence of GreA, we observed short- and long-lived RP_{ITC} states (Fig. 4 *B*, *D*, *F*, and *H*). The lifetimes of RP_{ITC} states (n = 216) are summarized in a histogram fitted with a double exponential, in which ∼60% of events were short-lived ($\tau = 340 \pm 60$ s, SEM) and ∼40% were long-lived ($\tau = 4{,}600 \pm 2{,}700$ s, SEM; Fig. 4*H*, blue; fractions based on quadrant analysis as discussed in Fig. 3 legend). Correlating these lifetimes with DNA bubble sizes (representing distinct RP_{ITC} states; Fig. 4 *A*, *D*, and *F* and accompanying legend) revealed that short-lived RP_{ITC} states are characterized by a Gaussian distribution of transcription bubble sizes with a mean apparent unwinding of 15.9 ± 0.4 bp (SEM) and a SD of 3.6 ± 0.4 bp, whereas long-lived events display two distinct states of apparent unwinding: a 20% fraction with mean apparent unwinding of only 9.9 ± 0.3 bp (SEM) and a SD of 0.7 ± 0.3 bp (SEM) and an 80% fraction with mean apparent unwinding of 14.8 ± 0.4 bp (SEM) and a SD of 2.3 ± 0.4 bp (SEM).

These data suggested that, in addition to the well-characterized RP_{ITC} state (Fig. 4*A*), a large fraction of RNAP complexes entered a distinct, long-lived state characterized by a smaller transcription bubble (denoted RP_{ITC}* in Fig. 4 *A*–*C*). We hypothesized that this long-lived initiation intermediate represented a backtracked RNAP that was characterized also in our quenched kinetics and gel-based transcription assays. If correct, the addition of GreA would be expected to markedly reduce the number of these long-lived events. In agreement, RP_{ITC} states (n = 209), observed in the presence of GreA, became uniformly short-lived ($\tau = 350 \pm 30$ s, SEM) and displayed a bubble size distribution similar to that observed for the short-lived RP_{ITC} states in the absence of GreA [16.2 ± 0.2 bp (SEM); SD 2 ± 0.2 bp (SEM); Fig. 4 *C*, *E*, *G*, and *H*]. The results shown in Fig. 4 followed transcription rounds of single RNAP molecules on immobilized DNA molecules carrying the lacCONS promoter sequence. These experiments were performed in the presence of the initiating dinucleotide used in the quenched kinetics assay (Figs. 1*D*, 2, and 3 and Figs. S3, S4, S8, and S9), A_pA. Additional magnetic tweezer transcription experiments using the lacCONS promoter with all NTPs in the absence of A_pA yielded similar trends to those in the presence of it (example of a trajectory in Fig. S10). Experiments conducted on a different promoter template (T5N25) at 100 μM each NTP also showed the same trends, which were furthermore independent of the presence (Fig. S11) or absence (Fig. S12) of the initiating dinucleotide of T5N25 promoter, A_pU. Specifically, we observed both short-lived RP_{ITC} states lasting tens of seconds and long-lived RP_{ITC}* states lasting thousands of seconds, for which the RP_{ITC}* state systematically displays a smaller mean unwinding amplitude with narrower distribution than the RP_{ITC} state. As observed for the lacCONS promoter, addition of GreA once again abrogates the minimally unwound, long-lived RP_{ITC}* state in favor of short-lived RP_{ITC} states with extensive unwinding and leading to highly efficient promoter escape.

Finally, we performed magnetic tweezer transcription experiments on the lacCONS promoter and at higher NTP concentrations (1 mM each NTP; no initiating dinucleotide), which resemble the concentrations of NTPs under normal physiological conditions. The results obtained in the absence of GreA (Fig. S13) continue to show long-lived RP_{ITC}* events that resemble the ones measured under lower NTP concentrations. The transcription initiation complexes formed at the lacCONS promoter in these conditions continue to display double-exponential lifetimes before bona fide escape and regular processive elongation: 84%

with a fast phase of only 91 ± 15 s (SEM) and 16% with a slow phase remaining in the thousands of seconds (Fig. S13).

In summary, the presence of GreA abrogates RP_{ITC}* states characterized by long lifetimes and smaller transcription bubbles in favor of RP_{ITC} states with short lifetimes and larger transcription bubbles, leading to highly efficient promoter escape (Figs. S11 and S12 *D* and *E*, quadrants, and S13*C*, quadrants). Hence, we conclude that GreA catalyzes the cleavage of nascent RNA transcript in backtracked complexes. The cleavage allows scrunching to resume so that the transcription bubble may reach its maximal size, efficiently driving the transition to a productive elongation. It also implies that the long-lived paused state is either caused by or stabilized through backtracking. These data further support the existence of a long-lived initiation state, in which the transcription bubble is smaller than its size in the presence of GreA, most likely due to backtracking. Altogether, the results provide evidence for the existence of the previously hypothesized paused and backtracked initiation state.

Conclusions

Our results support the existence of a previously hypothesized, yet uncharacterized, state in which RNAP backtracks and pauses during transcription initiation. We identified this paused–backtracked initiation intermediate under in vitro conditions with NTP concentrations that resemble physiological conditions (~100 μM to 1 mM). Moreover, GreA and NTP availability appear to play key roles in regulating the flux in or out of this state. Based upon these results, we propose a modified transcription initiation model (Fig. 5). The model proposes that transcription initiation is rate limiting not only due to multiple abortive cycles that can occur before transitioning into elongation (5, 31, 63, 70), but also due to the existence of a backtracked, paused state. Thus, we hypothesize the presence of two initiation pathways. If nascent RNA backtracks into the secondary channel, either RNAP can swiftly release it as an abortive product, if the hybrid is short enough (14, 35, 36), or the backtracked complex can be stabilized. The prolonged association of the backtracked transcript may lead to intrinsic (or GreA-induced) RNA cleavage by RNAP. The backtracked-paused complex may also slowly release the nascent RNA through further backtracking. The model depicted in Fig. 5 adds an additional "slow" pathway (red arrows and beige rectangle background) to the conventional abortive initiation model.

Although the paused–backtracked initiation intermediate was observed frequently even at high NTP concentration, its effect on transcription and promoter escape was most pronounced under limiting NTP concentrations. These findings could have direct implications for in vivo conditions. First, the intracellular concentrations of NTPs can vary by severalfold, even during normal bacterial growth from midlog to early stationary phase (68). Additionally, nutritional limitation (e.g., carbon sources) can lead to a significant decrease of intracellular NTPs that directly affect the efficiency of transcription initiation and start-site selection at promoters of ribosomal and pyrimidine biosynthetic operons [reviewed by Turnbough (69)]. Moreover, decreases in nucleotide pools become even more dramatic during metabolic stress induced by antibiotics, oxidative stress, etc. (67). Therefore, under certain growth and environmental conditions, NTP concentrations may become limiting and thus are likely to affect abortive synthesis, early transcription, pausing, and promoter escape. Second, a number of in vitro studies have shown that the rate-limiting steps in transcription initiation include promoter DNA recognition/binding, open complex formation, abortive RNA synthesis/release, and promoter escape, all of which are targets for regulation (53). In vivo analysis of the chromosomal distribution of bacterial RNAPs by ChIP-chip, ChIP-seq, and DNA footprinting demonstrated that even under normal growth conditions (without NTP deprivation), a substantial fraction of RNAP accumulated at promoters of both transcriptionally active and inactive regions, engaged in either "poised" or open promoter complexes or in initial transcribing and paused complexes (43, 71–74). These results indicate that abortive initiation and promoter escape are the major rate-limiting steps in vivo.

Mechanisms of transcription by cellular RNA polymerases are broadly conserved (75). For example, scrunching (3, 4, 76) and trigger loop function during catalysis (37, 77–80) are similar, as are some of the mechanistic roles of σ70 and TFIIB (1, 81). It will be important to determine whether similar backtracked states are adopted during transcription initiation by eukaryotic RNA polymerases. Mammalian RNA polymerase II (Pol II) pauses during early stages of transcription, and this represents a common regulatory intermediate (82). Potentially, a mechanistic intermediate of paused mammalian Pol II enzymes may involve RNA backtracking; such backtracked intermediates may help explain why TFIIS, a eukaryotic convergently evolved analog of GreA, has been linked to transcription initiation and assembles with Pol II at the promoter (42, 83, 84). Finally, we emphasize that, because RNAP transcription initiation is rate limiting at many genes and highly regulated in vivo, this previously hypothesized yet uncharacterized backtracked-paused RNAP state may lead to potential new strategies for molecular therapeutics and to the development of novel antibiotics.

Methods

Transcription Quenched Kinetics Assay.

Preparation of a stable RP_O, $RP_{ITC=2}$. RP_O solution is prepared with 3 μL *E. coli* RNAP holoenzyme (NEB, M0551S; 1.6 μM), 10 μL 2× transcription buffer [80 mM Hepes KOH, 100 mM KCl, 20 mM $MgCl_2$, 2 mM dithiotreitol (DTT), 2 mM 2-mercaptoethylamine-HCl (MEA), 200 μg/mL BSA, pH 7], 1 μL of 1 μM lacCONS (65) or T5N25 promoter (5) (sequence in Fig. 1*A* and Fig. S1), and 6 μL of water. RP_O is then incubated in solution at 37 °C for 30 min. To remove unreacted and nonspecifically bound RNAP, 1 μL of 100 mg/mL Heparin-Sepharose CL-6B beads (GE Healthcare) is added to RP_O solution together with 10 μL of prewarmed 1× transcription buffer [Heparin challenge (3, 65)]. The mixture is incubated for 1 min at 37 °C and centrifuged for at least 45 s at 6,000 rpm. A total of 20 μL of the supernatant containing RP_O is transferred into a new tube with initiating dinucleotide, for sP-DNA complexes (40–42). In this context, the Heparin-challenged RP_O solution is incubated with 1.5 μL of 10 mM adenylyl(3′–5′) adenosine or adenylyl(3′–5′) uridine (A_pA or A_pU; Ribomed) at 37 °C for 20 min to form stable $RP_{ITC=2}$ solution. This $RP_{ITC=2}$ solution is used as a stock for all transcription reactions (for more information regarding the use of initiating dinucleotides, see *Supporting Information*, *Initiating Dinucleotide With/Without a 5′-Triphosphate Group*). A total of 2 μL of RNase inhibitor (NEB; M0314S) is added into the $RP_{ITC=2}$ solution to prevent degradation of newly transcribed RNA molecules.

Design and measurement of the transcription kinetics. To produce runoff transcripts, high-purity ribonucleotide triphosphates (NTPs) (GE Healthcare) were used in all transcription reactions at 100 μM each. To obtain a specific initiation or elongation state, only a partial set of NTPs was used. The choice of the partial set of NTPs depended on the sequence of ITSs being used (Fig. 1*A* and Fig. S1). To exit from the initiation/elongation NTP-starved state the reaction mixture was complemented with all four NTPs. The nontemplate strands of all promoter DNAs have the sequence of 20 dA (20 consecutive A), the complementary sequence of ssDNA FRET probe (20 dT), at the end (Fig. 1*A* and Fig. S1 for probe target sequence). The ssDNA FRET probe is doubly end labeled with a pair of fluorophores suitable for smFRET: a donor, tetramethylrhodamine, at the 5′ end (5′ TAMRA modification) and an acceptor, Alexa Fluor 647, at the 3′ end (3′ Alexa Fluor 647 modification) [ordered from IDT (65)].

For kinetics, the reaction mixture is incubated with the partial set of NTPs for a constant duration of 40 min at 37 °C. All four NTPs are then added to the reaction mixture and incubated for various times, t_{exit}, at 37 °C. The reaction is quenched by addition of 0.5 M GndHCl. Subsequently, a ssDNA FRET probe is added to the quenched reaction mixture and incubated for 20 min at room temperature to detect runoff RNA transcripts produced during t_{exit} (see Fig. S6 for hybridization kinetics in 0.5M GndHCl). The quenched-probed reaction mixtures were then used for μsALEX measurements. An example of the quenched kinetic assay FRET results is shown in Fig. 1 *C* and *D*.

Each kinetic curve was measured in two or three separate repeats to show reproducibility (Fig. S7). The concentration of the ssDNA FRET probe in each

experimental repeat was designed so that the steady-state level of a kinetic curve would be 0.9 ± 0.05. To make all repeats of kinetic curves reach a steady-state level of exactly 0.9 and not close to it, these repeats had to be rescaled (as shown in Fig. S14 and a detailed explanation in *Supporting Information*, *RNAP–DNA Complex Concentration Adjustment and Rescaling for Transcription Kinetics Assays*).

Each time point in the quenched kinetics assay is measured for duration of 10–15 min, using a setup described in Panzeri et al. (85), using Perkin-Elmer SPADs and 532-nm and 638-nm CW lasers operating at powers of 170 μW and 80 μW, respectively.

For transcription kinetics experiments with GreA, 1 μM GreA is added to transcription complexes in NTP-starved initiation or elongation states and incubated for 15 min before adding all four NTPs to initiate transcription reactions for $\mathbf{t_{exit}}$.

Each kinetic measurement was performed at least in duplicates, using different preparations obtained on different days (Fig. S7). For each batch, we made sure of the following:

i) The FRET probe in the presence of transcription complexes without NTPs yielded a large high-FRET population with no or a negligible amount of low-FRET population (no NTP, negative control).

ii) After 20 min incubation of $RP_{ITC=2}$ with all four NTPs (steady state for $RP_{ITC=2}$; Figs. 1*D*, 2, and 3 *A* and *B* and Figs. S3, S4*A*, S7, S9, and S14), the fraction of hybridized probe reaches 90 ± 5% (positive control). This control is performed daily on the same batch used to prepare NTP-starved RNAP states.

iii) With an extralong incubation time (typically several hours) after quenching the reaction, the measurement yielded the same hybridized fraction as measured without the extra incubation (quenching does work).

The results of the negative control (no NTP) serve as the "t = 0" time point. The positive control shows that the prepared transcription complexes are active and produce a lower amount of transcripts than the detection limit of the assay (overall amount of transcripts is lower than the amount of ssDNA FRET probe) at very long times, "t = ∞."

All NTP-starved states were prepared from $RP_{ITC=2}$ stock solution. Because the other experimental conditions (concentrations, temperature, etc.) are identical, any changes in activity that may be caused solely due to the starvation of NTPs will show a change in the hybridized fraction in long time points of the kinetic trace. Such comparisons were routinely performed and have never shown a difference in the long time point baseline between the kinetics from $RP_{ITC=2}$ and from NTP-starved states (within 5% error). Therefore, we conclude that our experimental conditions (e.g., NTP starvation) did not alter the transcription activity but only the kinetics. In this regard, the same quantity of the stock solution could be used for kinetics assays for NTP-starved states as the one used for the abovementioned positive control.

μsALEX-smFRET data were analyzed as described in *Supporting Information*, *μsALEX-smFRET Analysis for the Quantification of Transcription Kinetics*.

Transcription Assays Visualizing Abortive Product Formation Using Urea-Denaturing PAGE Analysis of [^{32}P]-Radiolabeled RNA Products. Abortive transcription assays were run using the lacCONS promoter, having its probe target 20A sequence replaced by the WT lacUV5 sequence at registers from +20 to +39 (Fig. S8). Three units of RNAP holoenzyme (NEB; M0551S) was mixed with 50 nM promoter DNA in 1× transcription buffer in a final volume of 20 μL. The reaction was then incubated at 37 °C for 20 min to form RP_O, followed by addition of 1 μL of 100 mg/mL Heparin-Sepharose beads and 10 μL of transcription buffer. The mixture was incubated for ∼1 min and centrifuged, and 20 μL of the supernatant was removed and added to 10 μL prewarmed transcription buffer. After incubating an additional 10 min, A_pA was added at a final concentration of 1.3 mM and incubated for 30 min to form the $RP_{ITC=2}$. The $RP_{ITC=2}$ was then diluted to 400 μL with transcription buffer containing SUPERaseIN (AM2696; Thermo Fisher Scientific) to final concentrations of 1.7 nM template, 112 μM A_pA, and 0.3 units/μL SUPERaseIN. This solution was stored at room temperature and used as a stock for each time course.

For time-course experiments, 90 μL of the stock solution was briefly incubated to bring it to 37 °C. To analyze the production kinetics of abortive products from $RP_{ITC\leq7}$, stock solution was mixed with 10 μL of 200 μM UTP+GTP mixture supplemented with ∼10 μCi [α^{32}P]UTP. At each time point, 10 μL aliquot was then removed and mixed with an equal volume of formamide gel loading buffer. To analyze abortive product formation from RNAP that was not stalled, the UTP+GTP mixture was replaced by a complete set of NTPs. In experiments looking at the effects of GreA on abortive product formation, additional 15-min incubation at 37 °C was performed before the addition of NTPs, either in the presence or in the absence of 1 μM GreA. The stopped reaction aliquots were stored at −20 °C until running the urea-denaturing PAGE.

Samples were heated for 3 min at 90 °C and loaded on a 23% (wt/vol, 19:1 acrylamide:bis-acrylamide), 0.4-mm-thick urea-denaturing polyacrylamide gel. The gel usually ran for 5–6 h at 1,500 V in 1× TBE with an additional 0.3 M sodium acetate in the bottom well. The gels were then removed, dried, and exposed on a phosphor-storage screen about 2 d. Screens were visualized using a Typhoon PhosporImager.

Magnetic Trapping Assay.

Single-molecule experiments. For the single-molecule experiments we used the DNA constructs described in *Supporting Information*, *DNA Constructs for the Magnetic Trapping Assay*.

Functionalized 2.2-kbp DNA molecules were first attached to 1-μm-diameter streptavidin-coated magnetic beads (MyOne Streptavidin C1; Life Technologies) and then tethered to a modified glass capillary surface coated with anti-digoxigenin (Roche) (86). Experiments were carried out on a homemade magnetic tweezer microscope to extend and supercoil the DNA, running the PicoTwist software suite to track and analyze the position of the magnetic bead. This position marks the free end and thus the extension of the functionalized DNA. Data were analyzed using custom routines in the Xvin software suite. Experiments were carried out in standard buffer at 34 °C, using 100 pM RNAP saturated with σ70 (prepared as in ref. 87) and 100 μM A_pA (for experiments on lacCONS promoter) (we used 100 μM A_pU for experiments on T5N25 promoter) and 100 μM each of ATP, UTP, GTP, and CTP. When added, GreA is at 1 μM.

Raw time traces were filtered (∼1 s) for analysis. The lifetime of the initiation state is defined as the total time elapsed between initial promoter unwinding and the transition to promoter escape and formation of the elongation complex (RD_E). The extent of apparent unwinding is determined by averaging the DNA extension over the entire lifetime of the initiation state as defined above and taking the difference between this average extension and that observed in the baseline high-extension state that separates the succession of transcription events. Importantly, our analysis excluded unproductive transcription initiation events in which RNAP spontaneously dissociated from DNA without forming the elongation state RD_E. Finally, we note that all elongation complexes formed, whether from RP_{ITC} or RP_{ITC}*, displayed the expected elongation rate, namely ∼12 bases/s for 100 μM NTPs at 34 °C.

Interpretation of apparent DNA unwinding during scrunching and backtracking and its relation to the length of transcribed RNA as seen in the quenched kinetics assay. In the supercoiling transcription assay where plectonemic supercoils are present (+4 positive supercoils throughout), the extension changes of the DNA construct report on the number of supercoils. Specifically, the DNA typically contracts by ∼55 nm for every additional supercoil when extended at low force (F = 0.3 pN) as in these experiments. DNA unwinding by RNAP is sensitively reported via its effect on overall DNA supercoiling: Conservation of linking number means that topological unwinding of 10.5 bp results in an ∼55-nm decrease in DNA extension.

During initial transcription and scrunching, an "N-2" rule has been observed (88), relating the length of the RNA and the extent of DNA unwinding in the bubble. Because an RNA 2-mer can be formed in RPo without a need for additional DNA unwinding and scrunching, an RNA N-mer can be formed by additional unwinding and scrunching of N-2 bases. However, during backtracking, this linear relationship is lost, although the simplest hypothesis is that backtracking by 1 bp dehybridizes 1 bp of the RNA–DNA hybrid and reduces the bubble size by the same amount. Thus, in this work the single-molecule assay can report only on the apparent bubble size, which results from the final backtracked state. This measurement provides information complementary to that obtained from the quenched kinetics assay, which instead provides insight into the relation between accessible RNA lengths and likelihood of entry into a state that is not competent for promoter escape.

Separation of correlative lifetime/amplitude data into quadrants. We separate short- and long-lifetime initiation events by setting a boundary corresponding to the short mean lifetime plus 1 SD (as it is a single-exponential distribution this essentially means two times the short lifetime). We separate small and large bubbles by setting a boundary corresponding to the mean unwinding amplitude for the short-lifetime state in the absence of GreA plus 1 SD. Similar results are obtained if one uses the mean and SDs of amplitude data obtained in the +GreA condition and for which lifetime is homogeneously short. These boundaries determine the fractions of events categorized and cited as short or long lived and displaying small or large bubble sizes.

Illustrations. All illustrations of RNAP transcription initiation and elongation states have been prepared in Adobe Illustrator CC 2015.

Note Added in Proof. A study by Duchi et al. (89) that describes similar findings (but with much shorter paused initiation state), using somewhat different methodologies, was published while this manuscript was under final revisions.

ACKNOWLEDGMENTS. We thank Prof. William Gelbart, Prof. Charles Knobler, Dr. Cathy Yan Jin, and Xiyu Yi for fruitful discussions and Maya Lerner for preparation of illustrations. We thank Prof. Richard Ebright for generously providing us with the triphosphate dinucleotide pppApA, as a gift. The T.R.S. laboratory wishes to thank the CNRS, the University of Paris Diderot, and the Programme Equipe Labellisees of the French Ligue Contre le Cancer for core funding; this work was further made possible by ANR Grant "RepOne". This work was funded by the National Institutes of Health (Grant GM069709 to S. Weiss and Grant GM095904 to X.M. and S. Weiss) and the National Science Foundation (Grant MCB-1244175 to S. Weiss and D.J.T.).

1. Murakami KS, Darst SA (2003) Bacterial RNA polymerases: The wholo story. *Curr Opin Struct Biol* 13(1):31–39.
2. Young BA, Gruber TM, Gross CA (2002) Views of transcription initiation. *Cell* 109(4): 417–420.
3. Kapanidis AN, et al. (2006) Initial transcription by RNA polymerase proceeds through a DNA-scrunching mechanism. *Science* 314(5802):1144–1147.
4. Revyakin A, Liu C, Ebright RH, Strick TR (2006) Abortive initiation and productive initiation by RNA polymerase involve DNA scrunching. *Science* 314(5802):1139–1143.
5. Hsu LM (2002) Promoter clearance and escape in prokaryotes. *Biochim Biophys Acta* 1577(2):191–207.
6. Luse DS, Jacob GA (1987) Abortive initiation by RNA polymerase II in vitro at the adenovirus 2 major late promoter. *J Biol Chem* 262(31):14990–14997.
7. Carpousis AJ, Gralla JD (1980) Cycling of ribonucleic acid polymerase to produce oligonucleotides during initiation in vitro at the lac UV5 promoter. *Biochemistry* 19(14): 3245–3253.
8. Ellinger T, Behnke D, Bujard H, Gralla JD (1994) Stalling of Escherichia coli RNA polymerase in the +6 to +12 region in vivo is associated with tight binding to consensus promoter elements. *J Mol Biol* 239(4):455–465.
9. Hsu LM (2009) Monitoring abortive initiation. *Methods* 47(1):25–36.
10. Abbondanzieri EA, Shaevitz JW, Block SM (2005) Picocalorimetry of transcription by RNA polymerase. *Biophys J* 89(6):L61–L63.
11. Abbondanzieri EA, Greenleaf WJ, Shaevitz JW, Landick R, Block SM (2005) Direct observation of base-pair stepping by RNA polymerase. *Nature* 438(7067):460–465.
12. Adelman K, et al. (2002) Single molecule analysis of RNA polymerase elongation reveals uniform kinetic behavior. *Proc Natl Acad Sci USA* 99(21):13538–13543.
13. Wang MD, et al. (1998) Force and velocity measured for single molecules of RNA polymerase. *Science* 282(5390):902–907.
14. Epshtein V, et al. (2002) Swing-gate model of nucleotide entry into the RNA polymerase active center. *Mol Cell* 10(3):623–634.
15. Zhang G, et al. (1999) Crystal structure of Thermus aquaticus core RNA polymerase at 3.3 A resolution. *Cell* 98(6):811–824.
16. Hansen UM, McClure WR (1980) Role of the sigma subunit of Escherichia coli RNA polymerase in initiation. II. Release of sigma from ternary complexes. *J Biol Chem* 255(20):9564–9570.
17. Kapanidis AN, et al. (2005) Retention of transcription initiation factor sigma70 in transcription elongation: Single-molecule analysis. *Mol Cell* 20(3):347–356.
18. Korzheva N, Mustaev A, Nudler E, Nikiforov V, Goldfarb A (1998) Mechanistic model of the elongation complex of Escherichia coli RNA polymerase. *Cold Spring Harb Symp Quant Biol* 63:337–345.
19. Zuo Y, Steitz TA (2015) Crystal structures of the E. coli transcription initiation complexes with a complete bubble. *Mol Cell* 58(3):534–540.
20. Campagne S, Marsh ME, Capitani G, Vorholt JA, Allain FH (2014) Structural basis for -10 promoter element melting by environmentally induced sigma factors. *Nat Struct Mol Biol* 21(3):269–276.
21. Campbell EA, et al. (2002) Structure of the bacterial RNA polymerase promoter specificity sigma subunit. *Mol Cell* 9(3):527–539.
22. Mekler V, et al. (2002) Structural organization of bacterial RNA polymerase holoenzyme and the RNA polymerase-promoter open complex. *Cell* 108(5):599–614.
23. Murakami KS, Masuda S, Campbell EA, Muzzin O, Darst SA (2002) Structural basis of transcription initiation: An RNA polymerase holoenzyme-DNA complex. *Science* 296(5571):1285–1290.
24. Pupov D, Kuzin I, Bass I, Kulbachinskiy A (2014) Distinct functions of the RNA polymerase σ subunit region 3.2 in RNA priming and promoter escape. *Nucleic Acids Res* 42(7):4494–4504.
25. Samanta S, Martin CT (2013) Insights into the mechanism of initial transcription in Escherichia coli RNA polymerase. *J Biol Chem* 288(44):31993–32003.
26. Lee DN, Landick R (1992) Structure of RNA and DNA chains in paused transcription complexes containing Escherichia coli RNA polymerase. *J Mol Biol* 228(3):759–777.
27. Nudler E, Avetissova E, Markovtsov V, Goldfarb A (1996) Transcription processivity: Protein-DNA interactions holding together the elongation complex. *Science* 273(5272):211–217.
28. Sidorenkov I, Komissarova N, Kashlev M (1998) Crucial role of the RNA:DNA hybrid in the processivity of transcription. *Mol Cell* 2(1):55–64.
29. Komissarova N, Kashlev M (1998) Functional topography of nascent RNA in elongation intermediates of RNA polymerase. *Proc Natl Acad Sci USA* 95(25):14699–14704.
30. Travers AA, Burgessrr (1969) Cyclic re-use of the RNA polymerase sigma factor. *Nature* 222(5193):537–540.
31. Straney DC, Crothers DM (1985) Intermediates in transcription initiation from the E. coli lac UV5 promoter. *Cell* 43(2 Pt 1):449–459.
32. Krummel B, Chamberlin MJ (1989) RNA chain initiation by Escherichia coli RNA polymerase. Structural transitions of the enzyme in early ternary complexes. *Biochemistry* 28(19):7829–7842.
33. Straney DC, Crothers DM (1987) A stressed intermediate in the formation of stably initiated RNA chains at the Escherichia coli lac UV5 promoter. *J Mol Biol* 193(2): 267–278.
34. Hsu LM, et al. (2006) Initial transcribed sequence mutations specifically affect promoter escape properties. *Biochemistry* 45(29):8841–8854.
35. Weixlbaumer A, Leon K, Landick R, Darst SA (2013) Structural basis of transcriptional pausing in bacteria. *Cell* 152(3):431–441.
36. Martinez-Rucobo FW, Cramer P (2013) Structural basis of transcription elongation. *Biochim Biophys Acta* 1829(1):9–19.
37. Bar-Nahum G, et al. (2005) A ratchet mechanism of transcription elongation and its control. *Cell* 120(2):183–193.
38. Foster JE, Holmes SF, Erie DA (2001) Allosteric binding of nucleoside triphosphates to RNA polymerase regulates transcription elongation. *Cell* 106(2):243–252.
39. Holmes SF, Erie DA (2003) Downstream DNA sequence effects on transcription elongation. Allosteric binding of nucleoside triphosphates facilitates translocation via a ratchet motion. *J Biol Chem* 278(37):35597–35608.
40. Nedialkov YA, et al. (2003) NTP-driven translocation by human RNA polymerase II. *J Biol Chem* 278(20):18303–18312.
41. Sousa R (2001) A new level of regulation in transcription elongation? *Trends Biochem Sci* 26(12):695–697.
42. Guglielmi B, Soutourina J, Esnault C, Werner M (2007) TFIIS elongation factor and Mediator act in conjunction during transcription initiation in vivo. *Proc Natl Acad Sci USA* 104(41):16062–16067.
43. Reppas NB, Wade JT, Church GM, Struhl K (2006) The transition between transcriptional initiation and elongation in E. coli is highly variable and often rate limiting. *Mol Cell* 24(5):747–757.
44. Borukhov S, Lee J, Laptenko O (2005) Bacterial transcription elongation factors: New insights into molecular mechanism of action. *Mol Microbiol* 55(5):1315–1324.
45. Toulmé F, et al. (2000) GreA and GreB proteins revive backtracked RNA polymerase in vivo by promoting transcript trimming. *EMBO J* 19(24):6853–6859.
46. Brodolin K, Zenkin N, Mustaev A, Mamaeva D, Heumann H (2004) The sigma 70 subunit of RNA polymerase induces lacUV5 promoter-proximal pausing of transcription. *Nat Struct Mol Biol* 11(6):551–557.
47. Shaevitz JW, Abbondanzieri EA, Landick R, Block SM (2003) Backtracking by single RNA polymerase molecules observed at near-base-pair resolution. *Nature* 426(6967): 684–687.
48. Stepanova E, et al. (2007) Analysis of promoter targets for Escherichia coli transcription elongation factor GreA in vivo and in vitro. *J Bacteriol* 189(24):8772–8785.
49. Stepanova E, Wang M, Severinov K, Borukhov S (2009) Early transcriptional arrest at Escherichia coli rplN and ompX promoters. *J Biol Chem* 284(51):35702–35713.
50. Feng GH, Lee DN, Wang D, Chan CL, Landick R (1994) GreA-induced transcript cleavage in transcription complexes containing Escherichia coli RNA polymerase is controlled by multiple factors, including nascent transcript location and structure. *J Biol Chem* 269(35):22282–22294.
51. Hsu LM, Vo NV, Chamberlin MJ (1995) Escherichia coli transcript cleavage factors GreA and GreB stimulate promoter escape and gene expression in vivo and in vitro. *Proc Natl Acad Sci USA* 92(25):11588–11592.
52. Borukhov S, Sagitov V, Goldfarb A (1993) Transcript cleavage factors from E. coli. *Cell* 72(3):459–466.
53. Hsu LM (2008) Promoter escape by Escherichia coli RNA polymerase. *Ecosal Plus* 3(1).
54. Goldman SR, Ebright RH, Nickels BE (2009) Direct detection of abortive RNA transcripts in vivo. *Science* 324(5929):927–928.
55. Skancke J, Bar N, Kuiper M, Hsu LM (2015) Sequence-dependent promoter escape efficiency is strongly influenced by bias for the pretranslocated state during initial transcription. *Biochemistry* 54(28):4267–4275.
56. Kapanidis AN, et al. (2004) Fluorescence-aided molecule sorting: Analysis of structure and interactions by alternating-laser excitation of single molecules. *Proc Natl Acad Sci USA* 101(24):8936–8941.
57. Kapanidis AN, et al. (2005) Alternating-laser excitation of single molecules. *Acc Chem Res* 38(7):523–533.
58. Förster T (1948) Zwischenmolekulare Energiewanderung Und Fluoreszenz. *Ann Phys* 2(1-2):55–75.
59. Deniz AA, et al. (1999) Single-pair fluorescence resonance energy transfer on freely diffusing molecules: Observation of Förster distance dependence and subpopulations. *Proc Natl Acad Sci USA* 96(7):3670–3675.
60. Deniz AA, et al. (2001) Ratiometric single-molecule studies of freely diffusing biomolecules. *Annu Rev Phys Chem* 52:233–253.
61. Mekler V, Pavlova O, Severinov K (2011) Interaction of Escherichia coli RNA polymerase σ70 subunit with promoter elements in the context of free σ70, RNA polymerase holoenzyme, and the β′-σ70 complex. *J Biol Chem* 286(1):270–279.
62. Mekler V, Minakhin L, Kuznedelov K, Mukhamedyarov D, Severinov K (2012) RNA polymerase-promoter interactions determining different stability of the Escherichia coli and Thermus aquaticus transcription initiation complexes. *Nucleic Acids Res* 40(22):11352–11362.
63. Margeat E, et al. (2006) Direct observation of abortive initiation and promoter escape within single immobilized transcription complexes. *Biophys J* 90(4):1419–1431.
64. Mukhopadhyay J, et al. (2001) Translocation of sigma(70) with RNA polymerase during transcription: Fluorescence resonance energy transfer assay for movement relative to DNA. *Cell* 106(4):453–463.
65. Kim S, et al. (2011) High-throughput single-molecule optofluidic analysis. *Nat Methods* 8(3):242–245.

66. Laptenko O, Lee J, Lomakin I, Borukhov S (2003) Transcript cleavage factors GreA and GreB act as transient catalytic components of RNA polymerase. *EMBO J* 22(23): 6322–6334.
67. Belenky P, et al. (2015) Bactericidal antibiotics induce toxic metabolic perturbations that lead to cellular damage. *Cell Reports* 13(5):968–980.
68. Buckstein MH, He J, Rubin H (2008) Characterization of nucleotide pools as a function of physiological state in Escherichia coli. *J Bacteriol* 190(2):718–726.
69. Turnbough CL, Jr (2008) Regulation of bacterial gene expression by the NTP substrates of transcription initiation. *Mol Microbiol* 69(1):10–14.
70. Tang GQ, Roy R, Ha T, Patel SS (2008) Transcription initiation in a single-subunit RNA polymerase proceeds through DNA scrunching and rotation of the N-terminal subdomains. *Mol Cell* 30(5):567–577.
71. Herring CD, et al. (2005) Immobilization of Escherichia coli RNA polymerase and location of binding sites by use of chromatin immunoprecipitation and microarrays. *J Bacteriol* 187(17):6166–6174.
72. Grainger DC, Hurd D, Harrison M, Holdstock J, Busby SJ (2005) Studies of the distribution of Escherichia coli cAMP-receptor protein and RNA polymerase along the *E. coli* chromosome. *Proc Natl Acad Sci USA* 102(49):17693–17698.
73. Kusuya Y, Kurokawa K, Ishikawa S, Ogasawara N, Oshima T (2011) Transcription factor GreA contributes to resolving promoter-proximal pausing of RNA polymerase in Bacillus subtilis cells. *J Bacteriol* 193(12):3090–3099.
74. Hatoum A, Roberts J (2008) Prevalence of RNA polymerase stalling at Escherichia coli promoters after open complex formation. *Mol Microbiol* 68(1):17–28.
75. Werner F, Grohmann D (2011) Evolution of multisubunit RNA polymerases in the three domains of life. *Nat Rev Microbiol* 9(2):85–98.
76. Fazal FM, Meng CA, Murakami K, Kornberg RD, Block SM (2015) Real-time observation of the initiation of RNA polymerase II transcription. *Nature* 525(7568):274–277.
77. Allison LA, Moyle M, Shales M, Ingles CJ (1985) Extensive homology among the largest subunits of eukaryotic and prokaryotic RNA polymerases. *Cell* 42(2):599–610.
78. Hekmatpanah DS, Young RA (1991) Mutations in a conserved region of RNA polymerase II influence the accuracy of mRNA start site selection. *Mol Cell Biol* 11(11): 5781–5791.
79. Thuillier V, Brun I, Sentenac A, Werner M (1996) Mutations in the alpha-amanitin conserved domain of the largest subunit of yeast RNA polymerase III affect pausing, RNA cleavage and transcriptional transitions. *EMBO J* 15(3):618–629.
80. Weilbaecher R, Hebron C, Feng G, Landick R (1994) Termination-altering amino acid substitutions in the beta' subunit of Escherichia coli RNA polymerase identify regions involved in RNA chain elongation. *Genes Dev* 8(23):2913–2927.
81. Sainsbury S, Niesser J, Cramer P (2013) Structure and function of the initially transcribing RNA polymerase II-TFIIB complex. *Nature* 493(7432):437–440.
82. Adelman K, Lis JT (2012) Promoter-proximal pausing of RNA polymerase II: Emerging roles in metazoans. *Nat Rev Genet* 13(10):720–731.
83. Kim B, et al. (2007) The transcription elongation factor TFIIS is a component of RNA polymerase II preinitiation complexes. *Proc Natl Acad Sci USA* 104(41):16068–16073.
84. Stepanova EV, Shevelev AB, Borukhov SI, Severinov KV (2009) Mechanisms of action of RNA polymerase-binding transcription factors that do not bind to DNA. *Biofizika* 54(5):773–790.
85. Panzeri F, et al. (2013) Single-molecule FRET experiments with a red-enhanced custom technology SPAD. *Proc SPIE Int Soc Opt Eng*, 8590.
86. Revyakin A, Ebright RH, Strick TR (2005) Single-molecule DNA nanomanipulation: Improved resolution through use of shorter DNA fragments. *Nat Methods* 2(2): 127–138.
87. Howan K, et al. (2012) Initiation of transcription-coupled repair characterized at single-molecule resolution. *Nature* 490(7420):431–434.
88. Revyakin A, Ebright RH, Strick TR (2004) Promoter unwinding and promoter clearance by RNA polymerase: Detection by single-molecule DNA nanomanipulation. *Proc Natl Acad Sci USA* 101(14):4776–4780.
89. Duchi D, et al. (2016) RNA polymerase pausing during initial transcription. *Mol Cell* 63(6):939–950.

Supporting Information

Lerner et al. 10.1073/pnas.1605038113

Rationale of the Single-Round Character of the Quenched Kinetics Transcription Assay

Transcription reaction kinetics were measured after adding all NTPs at saturating concentrations. Theoretically, after RNAP runs off the DNA and dissociates from it, it may rebind promoter DNA, form another open transcription bubble and initiate another round of transcription. This would result in kinetic curves that do not reach a steady-state plateau, because transcripts may be produced multiple times by the same enzyme. After fast rebinding of the σ70 subunit with the core RNAP to form the RNAP holoenzyme ($K_d = 0.26$ nM) (1), the binding affinity of RNAP holoenzyme to promoter DNA is relatively low ($K_d \sim 100$ nM at biologically relevant pH and ionic strength). Following the findings of Ko and Heyduk (2), holoenzyme rebinding to promoter DNA results in formation of an open transcription bubble in 5–10 min at RNAP concentration of 75 nM; because RNAP concentrations used in our assay are less than 1 nM, this rate should be ∼50 times slower. Therefore, the potential effects of multiround transcription would be observed in our experimental conditions only after 250–500 min. We recorded kinetic curves that reach steady-state plateaus (FRET probes hybridized to transcripts) that did not increase within our experimental timeframe (up to 120 min). Furthermore, the steady-state plateaus did not exceed 90 ± 5% of the overall level of FRET ssDNA probe (i.e., the plateau was not simply a consequence of saturation of FRET probes).

Initiating Dinucleotide With/Without a 5′-Triphosphate Group

To avoid potential alternative transcription start-site selection (3, 4), we used initiating dinucleotides (A_pA or A_pU in the case of lacCONS or T5N25 promoters, respectively) as primers for correct positioning of transcription initiation. As proposed by Kapanidis et al. (5) and also shown here (Fig. S2), measurements of transcription bubble conformation indicate that dinucleotides stabilize the transcription bubble in vitro. Moreover, initiating RNA primers reduce the start-site heterogeneity and minimize RNAP diversion into an unproductive pathway (6–8). However, commercially available dinucleotide primers are synthesized in the form of base-phosphate-base and hence do not have a 5′-triphosphate group. This, in turn, leads to RNA transcripts with a 5′-hydroxyl group, instead of a 5′-triphosphate group.

Exit kinetics out of NTP-starved $RP_{ITC\leq 7}$, formed using $_{ppp}A_pA$ (generously provided by Richard Ebright, Rutgers University, Piscataway, NJ), instead of A_pA, resulted in a large kinetic delay relative to exit kinetics out of $RP_{ITC=2}$ (Fig. S3), similar to the same delay when A_pA was used (Figs. 2 and 3*A*). In addition, the results of magnetic tweezers experiments using only the regular NTPs (without A_pA or A_pU, for lacCONS or T5N25 promoters, respectively) demonstrated a similar paused–backtracked state in initiation, as when using A_pA (Figs. S10 and S12).

Difficulties in the Measurement of Single-Run Transcription Runoff Kinetics Using Gel-Based Ensemble Assays

Kinetic measurements using the quenched-kinetics hybridizing FRET probe (such as those presented in this work) could be performed, in principle, at the (high concentration) ensemble level by incorporating a radioactive label and quenching the reaction at different time points. The quantity of runoff products at each time point could then be determined by running the reactions by a denaturing PAGE and quantified by autoradiography. These gel-based assays, however, are time-consuming and produce more variable results than the smFRET assays. Moreover, it is extremely challenging to visualize runoff transcripts with small sizes at low concentration due to low signal-to-noise ratio. We were unable to use this approach because this was the exact condition [i.e., detection of small transcripts (39 nt or 41 nt) at the single-round reaction level] we sought to investigate. To increase the signal, higher constituent concentrations could be used, but at the risk of running the transcription assays at multiple-round, rather than single-round conditions. Unfortunately, multiple-round conditions alter the process kinetics and, therefore, cannot produce reliable data. As an alternative, the concentration ratio of radiolabeled NTP to unlabeled NTPs could be increased to promote the incorporation of radiolabeled NTP, thereby achieving high signal-to-noise ratio. However, in this case, the total concentration of NTPs has to be significantly dropped because the radiolabeled NTP is limiting. This would lead to a significant deviation from biologically relevant conditions and the conditions used in the smFRET based assays. Precise quantification of product concentration at different time points requires that the concentrations of RNAP and promoter DNA in the reactions are kept low, in such a way that each preformed open complex would produce only one runoff transcript after the addition of NTPs. Single-round reactions, in turn, require highly sensitive and accurate detection of very low concentrations of product RNA molecules.

RNAP–DNA Complex Concentration Adjustment and Rescaling for Transcription Kinetics Assays

The exact concentration of catalytically competent RNAP–promoter DNA complexes in the prepared stock solution is unknown for the following reasons: (*i*) Not all RNAPs successfully bind to the promoter DNA and form transcriptionally competent complexes. (*ii*) Unreacted and nonspecifically bound RNAPs are eliminated in the Heparin challenge step. (*iii*) The activity of RNAP–promoter complexes could vary with conditions. Therefore, the amount of the stock solution added in the reaction mixtures for kinetic assays is calibrated beforehand to yield a low-FRET population fraction of 0.90 ± 0.05 at the steady state (20 min for $RP_{ITC=2}$). In other words, the concentrations of RNAP–DNA complexes in the reaction mixture were adjusted to produce transcripts whose quantity is 90 ± 5% of the detection limit at the steady state. In most cases, RNAP–DNA complexes used for kinetic assays were more than 50 times diluted from the prepared stock solutions. Despite the concentration adjustment, different repeats yield steady-state values with small deviations around 0.9 (±0.05; Fig. S14). Repetitions of the same experiments are used to report on the averaged kinetics as well as the correct statistical deviations from them. For that purpose, the kinetic curves of experimental repetitions have to be standardized to the same steady-state level. To do so, we applied rescaling factors for all repetitions of kinetic curves so that all of them reach a steady-state level of 0.9 (Fig. S14).

The results shown in Figs. 1*D*, 2, 3*A*, and 3*B* and Figs. S3, S4, and S9 are all averages of such rescaled–repeated measurements (examples of these repeats are shown in Figs. S7 and S14). The error bars reported in these figures are the SD following the averaging of repeated measurements.

μsALEX-smFRET Analysis for the Quantification of Transcription Kinetics

Dual-color fluorescence photon timestamps from freely diffusing molecules are recorded using an ALEX-FAMS setup (9, 10). Fluorescence bursts are identified in the recorded stream of photon timestamps, and the number of photons in a burst and the burst start/stop times are tabulated. Each burst is identified using

a sliding-window burst search that looks for consecutive m(= 10) photons exhibiting a count rate higher than a given threshold parameter F(= 6) times the background rate (11, 12). The background rate is estimated as a function of time (typically over time durations of 30 s) via maximum-likelihood fitting of the interphoton delays distribution. This ensures that slow changes in the background rate are accounted for. In single-molecule μsALEX analysis, three streams of photons are analyzed: donor and acceptor fluorescence photons during green laser excitation (noted here as DD and DA, respectively) and acceptor photons during red laser excitation (noted here as AA). Burst photon counts in each of these photon streams are background corrected by subtracting the burst duration times the background rate. First, an all-photon (all streams) burst search is applied. After filtering for bursts with sizes larger than 25 photons, the proximity ratio and the stoichiometry are calculated for each burst to identify the subpopulation of bursts where both donor and acceptor are active (FRET subpopulation), the subpopulation of donor-only fluorescence bursts (DO), and the subpopulation of acceptor-only fluorescence bursts (AO) (13). Next, correction factors are calculated according to Lee et al. (13). These correction factors include the donor fluorescence leakage into the acceptor detection channel (lk ~ 0.07), a factor that accounts for acceptors directly excited by the green laser (dir ~ 0.04), and the factor correcting for differences in donor and acceptor quantum yields and detection efficiencies ($\gamma \sim 0.61$).

Next, a dual-channel burst search (DCBS) (intersection of bursts from green excitation burst search and red excitation burst search) (14) is performed using m = 10 and F = 6, to isolate the FRET-only subpopulation for further analysis. After all correction factors are applied, the following two conditions are used to isolate smFRET data (on results of DCBS with m = 10 and F = 6):

i) $(n_{DA} - lk \cdot n_{DD} - dir \cdot n_{AA}) + \gamma \cdot n_{DD} \geq 25$
ii) $n_{AA} \geq 25$.

Each transcription quenched kinetics time point consists of the same two FRET populations but with different fractions that follow the evolution of the runoff transcript production (Fig. 1 *C* and *D*). All corrected FRET histograms of all time points in a given kinetic trace are globally fitted to a sum of two Gaussians. In the context of the global model, the means and widths of the subpopulations are constrained to be constant as a function of time (i.e., the same for all datasets), whereas the amplitudes are left free to vary for each time point.

Control measurements were carried out to show the stabilizing effect of the initiating dinucleotide, A_pA, on the open transcription bubble (Fig. S2) as well as characterize the effect of 0.5 M GndHCl as a quencher of the transcription reaction (Fig. S5*B*). These were μsALEX-smFRET measurements detecting fluorescence from donor and acceptor dyes internally labeling bases in the transcription bubble in initiation [NT(−8)ATTO647N—T(−5)ATTO550 (purchased from IBA); illustration in Fig. S5*B*] in the lacCONS promoter DNA. The analysis of bursts for these measurements used the same burst search criteria as mentioned above (DCBS with m = 10 and F = 6), corrected for donor fluorescence leakage into the acceptor channel (lk ~ 0.065) and for acceptor direct excitation (dir ~ 0.055) and filtered for cases with donor-excitation size above 50 photons $[(n_{DA} - lk \cdot n_{DD} - dir \cdot n_{AA}) + n_{DD} \geq 50]$ and acceptor-excitation size above 50 photons $[n_{AA} \geq 50]$. In Fig. S2, the brightness of each burst (the burst size divided by its duration) shows the value accumulated in the FRET histogram, to account for possible differences in dye brightness and duration in the excitation beam for the molecules in each state. Then, the FRET histogram was normalized to present the data as a probability density function (PDF).

The background-dependent burst search and selection in this work were performed using FRETBursts, an open-source burst analysis program for smFRET data (15). Model fittings were performed using Matlab scripts (MathWorks Matlab) through the lsqcurvefit nonlinear regression function.

DNA Constructs for the Magnetic Trapping Assay

We designed and had custom-synthesized (Eurofins MWG) DNA fragments flanked by KpnI sites containing a modular region for insertion of a promoter and initial transcript, followed by a transcribed region and a terminator. The modular region is flanked by HindIII and SpeI sites, 5′ GGTACCAAGCTTGCGAACTGCACTCGGAAC**ACTAGT**ATGCATCGAATAGCCATCCCAATCGATATCGAGGAGTTTAAATATGGCTGATGCATGAATTCGTTAATAACAGGCCTGCTGGTAATCGCAGGCCTTTTTATTTGGGAATTCGGTACC, where KpnI sites are indicated in red, HindIII and SpeI sites are underlined, and the tR2 terminator is in purple. This transcription backbone was cloned into the KpnI site of the *Thermus aquaticus* RPOC gene, and a 2.2-kbp subfragment of this construct centered about the transcription unit was PCR amplified and subcloned into the XbaI and SbfI sites of pUC18, using HiFi thermostable polymerase (Roche) and PCR primers (XbaI and SbfI sites underlined): 5′ GAGAGATCTAGAGACCTTCTGGATCTCGTCCACCAGG and 5′ GAGAGACCTGCAGGACATCAAGGACGAGGTGTGG.

We then cloned the lacCONS promoter into the HindIII and SpeI sites underlined above, using the oligo-based dsDNA fragment with the top strand: 5′ AGCTAGGCTTGACACTTTATGCTTCGGCTCGTATAATGTGTGGAATTGTGAGAGCGGATTAG.

Similarly, we cloned the T5N25 promoter, using the dsDNA fragment with the following top strand: 5′ AGCTAAAAATTTATTTGCTTTCAGGAAAATTTTTCTGTATAATAGATTCATAAATTTGAGAGAGGAGTCC.

DNA for single-molecule experiments was prepared from freshly grown DH5α by ion-exchange chromatography (Macherey-Nagel) and digested with XbaI and SbfI, and the 2.2-kb band was isolated by gel purification and extraction, using a spin column (Macherey-Nagel).

The 2.2-kbp DNA fragments containing the centrally located transcription unit were ligated at the XbaI site to 1 kbp DNA multiply labeled with biotin and at the SbfI site to 1 kbp DNA multiply labeled with digoxigenin. Labeled DNAs were synthesized via PCR carried out in the presence of dUTP-biotin and dUTP-digoxigenin, respectively (Roche) (16, 17).

1. Maeda H, Fujita N, Ishihama A (2000) Competition among seven Escherichia coli sigma subunits: Relative binding affinities to the core RNA polymerase. *Nucleic Acids Res* 28(18):3497–3503.
2. Ko J, Heyduk T (2014) Kinetics of promoter escape by bacterial RNA polymerase: Effects of promoter contacts and transcription bubble collapse. *Biochem J* 463(1):135–144.
3. Winkelman JT, et al. (2016) Multiplexed protein-DNA cross-linking: Scrunching in transcription start site selection. *Science* 351(6277):1090–1093.
4. Robb NC, et al. (2013) The transcription bubble of the RNA polymerase-promoter open complex exhibits conformational heterogeneity and millisecond-scale dynamics: Implications for transcription start-site selection. *J Mol Biol* 425(5):875–885.
5. Kapanidis AN, et al. (2006) Initial transcription by RNA polymerase proceeds through a DNA-scrunching mechanism. *Science* 314(5802):1144–1147.
6. Kubori T, Shimamoto N (1996) A branched pathway in the early stage of transcription by Escherichia coli RNA polymerase. *J Mol Biol* 256(3):449–457.
7. Susa M, Sen R, Shimamoto N (2002) Generality of the branched pathway in transcription initiation by Escherichia coli RNA polymerase. *J Biol Chem* 277(18): 15407–15412.
8. Stepanova E, Wang M, Severinov K, Borukhov S (2009) Early transcriptional arrest at Escherichia coli rplN and ompX promoters. *J Biol Chem* 284(51):35702–35713.
9. Kapanidis AN, et al. (2005) Alternating-laser excitation of single molecules. *Acc Chem Res* 38(7):523–533.
10. Kapanidis AN, et al. (2004) Fluorescence-aided molecule sorting: Analysis of structure and interactions by alternating-laser excitation of single molecules. *Proc Natl Acad Sci USA* 101(24):8936–8941.
11. Michalet X, et al. (2013) Development of new photon-counting detectors for single-molecule fluorescence microscopy. *Philos Trans R Soc B* 368(1611):20120035.
12. Eggeling C, et al. (2001) Data registration and selective single-molecule analysis using multi-parameter fluorescence detection. *J Biotechnol* 86(3):163–180.

13. Lee NK, et al. (2005) Accurate FRET measurements within single diffusing biomolecules using alternating-laser excitation. *Biophys J* 88(4):2939–2953.
14. Nir E, et al. (2006) Shot-noise limited single-molecule FRET histograms: Comparison between theory and experiments. *J Phys Chem B* 110(44):22103–22124.
15. Ingargiola A, Lerner E, Chung S, Weiss S, Michalet X (2016) FRETBursts: An Open Source Toolkit for Analysis of Freely-Diffusing Single-Molecule FRET. *Plos One* 11(8):e0160716.
16. Revyakin A, Ebright RH, Strick TR (2004) Promoter unwinding and promoter clearance by RNA polymerase: Detection by single-molecule DNA nanomanipulation. *Proc Natl Acad Sci USA* 101(14):4776–4780.
17. Revyakin A, Ebright RH, Strick TR (2005) Single-molecule DNA nanomanipulation: Improved resolution through use of shorter DNA fragments. *Nat Methods* 2(2): 127–138.

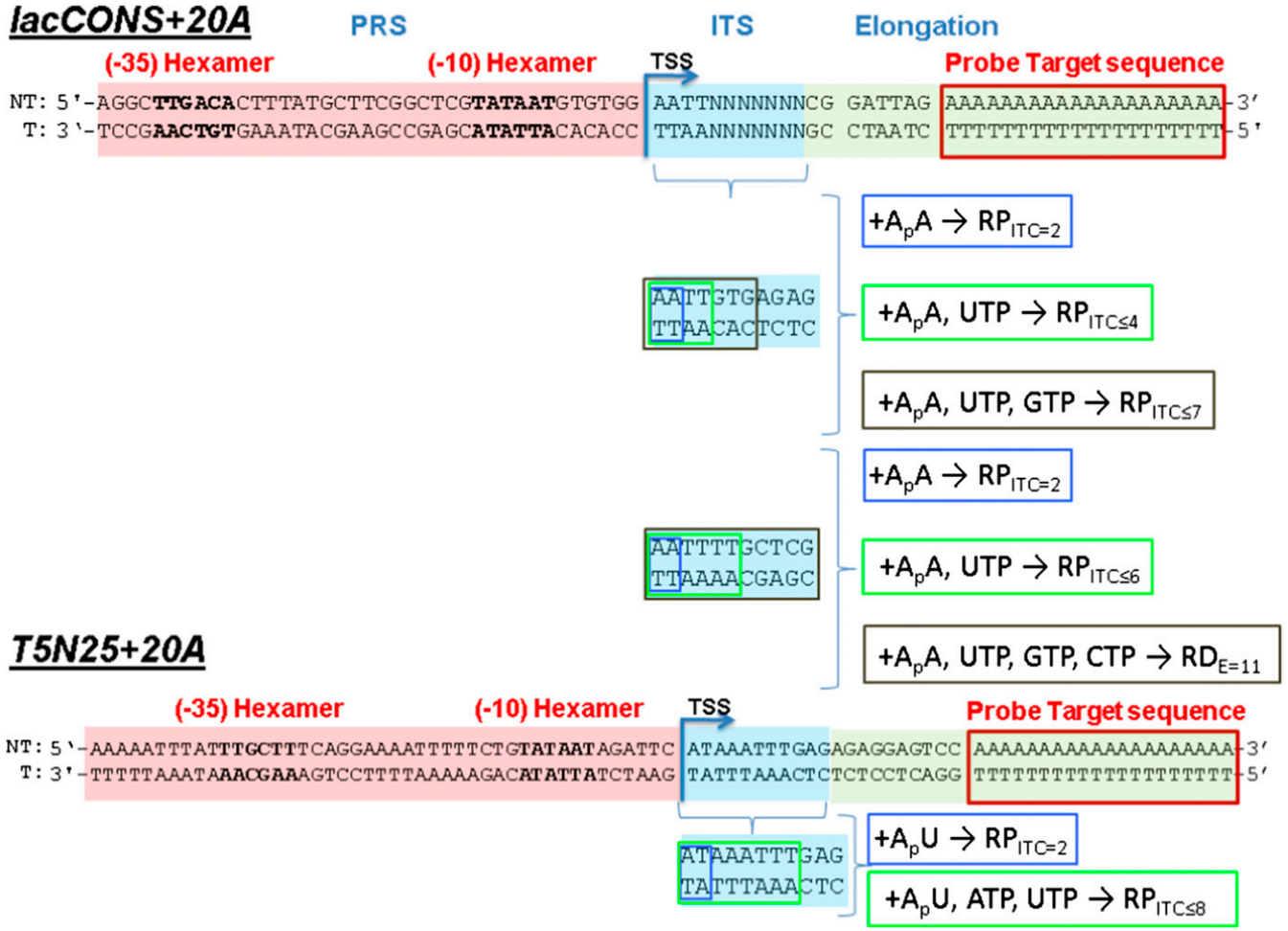

Fig. S1. lacCONS and T5N25 promoter sequences used in transcription runoff kinetics. Shown are the sequences of lacCONS (*Top*) and T5N25 (*Bottom*) promoters used in the quenched kinetics assays. Highlighted are the PRS (pink), the TSS (blue arrow), the ITS (cyan), and the elongation sequence (yellow). The sequence of the elongation region contains a 20-dT stretch that transcribes into a 20-A stretch in the RNA, which is detected by the doubly labeled ssDNA FRET probe. The lacCONS+20A sequence represents each of the possible sequence variants indicated by the NNN designation in the ITS.

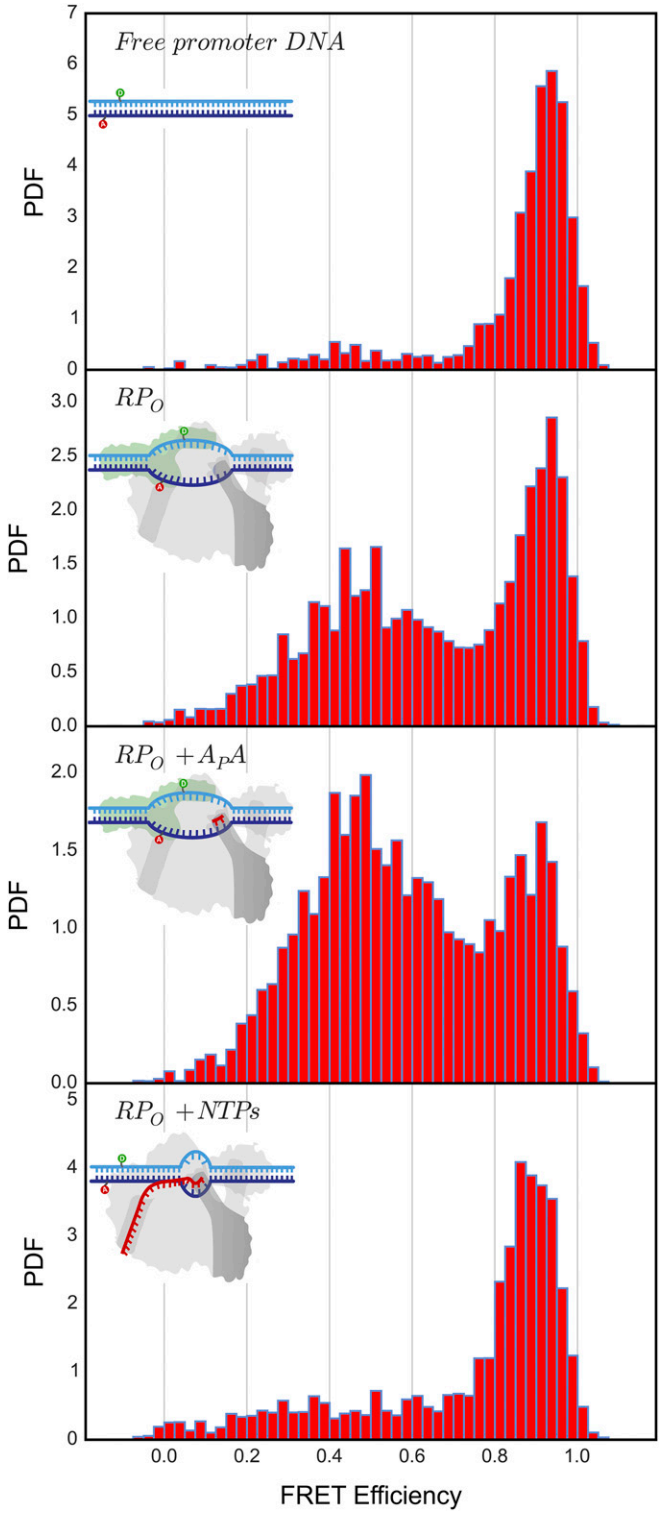

Fig. S2. A_pA stabilizes the open conformation of the transcription bubble in the lacCONS promoter. Shown is quantification of transcription bubble opening by smFRET. The higher FRET peak represents the annealed doubly labeled promoter DNA either in free form (and possibly the RP closed complex; *Top*) or after promoter escape (*Bottom*). The lower FRET peak(s) represent(s) the promoter DNA with an open bubble. (*Top* to *Bottom*) Panels show results for DNA only (free promoter DNA), RP_O, $RP_{ITC=2}$ ($RP_O + A_pA$), and runoff (RP_O + NTPs). In the presence of the initiating dinucleotide, A_pA, the relative proportion of the midFRET subpopulation increases in comparison with RP_O (i.e., in the absence of A_pA). This doubly labeled lacCONS promoter [NT(−8)ATTO647N—T(−5)ATTO550] shows bubble opening and promoter escape activities, as judged by the decrease in FRET efficiency in the presence of RNAP (distance between the dyes increases upon bubble formation and throughout initiation) and the increase back to high FRET upon addition of all NTPs (RNAP escapes promoter, and hence the RP complex, including the bubble, moves downstream, and the labeled DNA bases reanneal behind it). Each burst added to the FRET histogram is weighted by its brightness (the number of photons in a burst divided by the burst duration). The weighted FRET histogram is then normalized (hence the *y*-axis values follow the PDF).

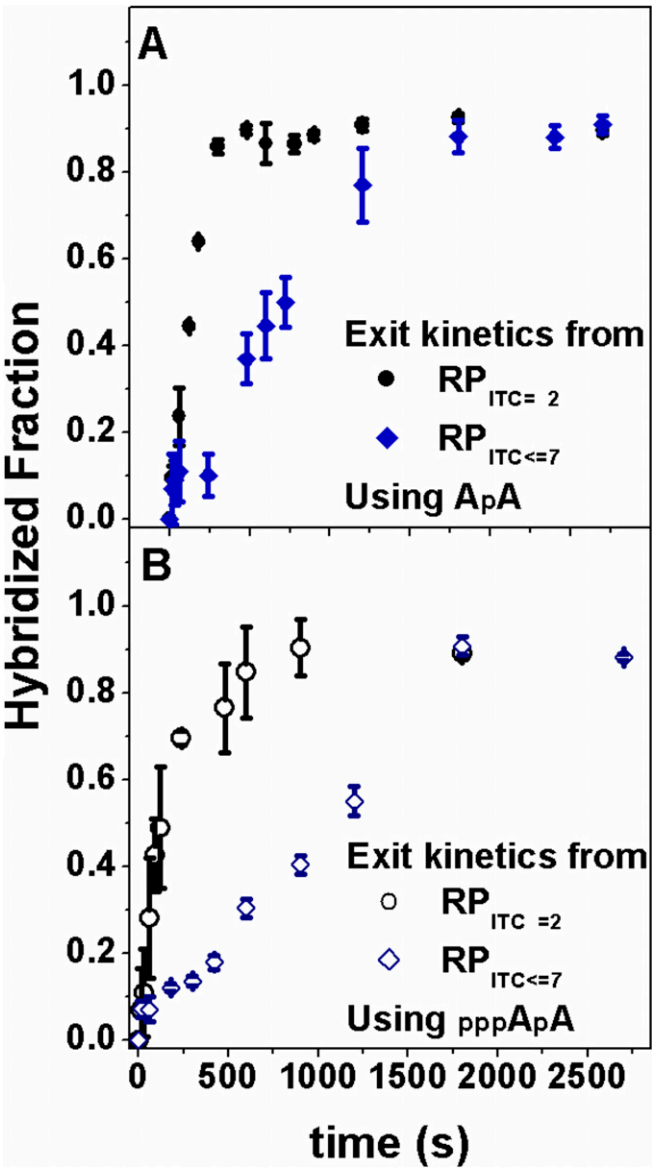

Fig. S3. Runoff kinetics yield similar results when using an initiating dinucleotide without or with a triphosphate. (*A* and *B*, respectively) Runoff kinetics starting from $RP_{ITC\leq 7}$ (blue) are slower than from $RP_{ITC=2}$ (black), when $RP_{ITC=2}$ was prepared by incubation with an initiating dinucleotide, either without (*A*) or with (*B*) a triphosphate.

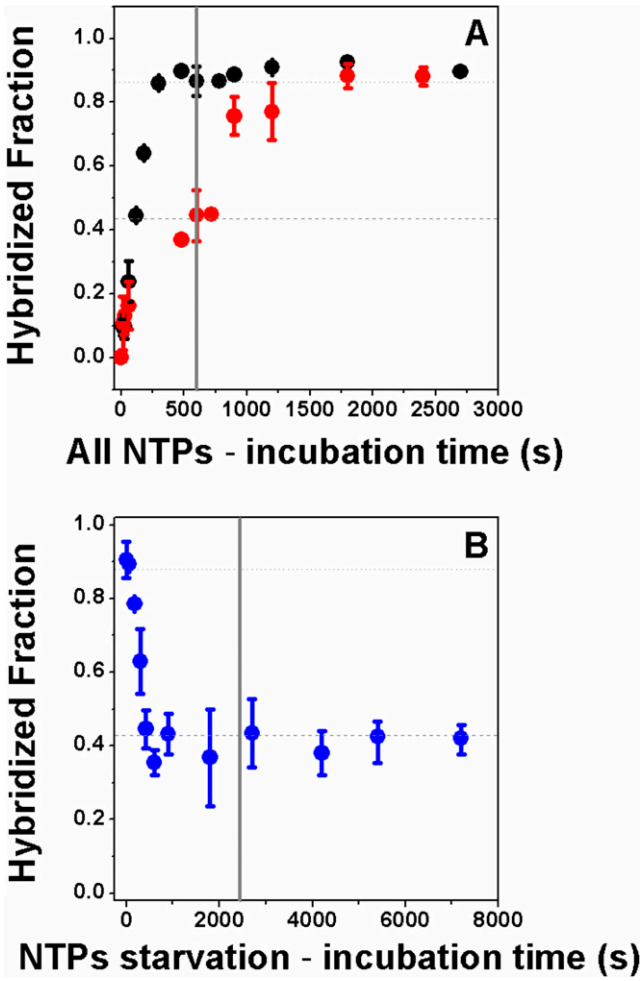

Fig. S4. Entrance into $RP_{ITC\leq 7}$ state occurs faster than the incubation times used. (*A*) Runoff kinetics starting from $RP_{ITC\leq 7}$ (red) or from $RP_{ITC=2}$ (black) when $RP_{ITC=2}$. Vertical gray line highlights the hybridization fraction of the RNA transcript with the FRET probe at a given incubation time with all NTPs, t_{exit} = 10 min, and these hybridization fractions are highlighted by dashed gray horizontal lines. (*B*) This condition (t_{exit} = 10 min) was used as a constant incubation time with all NTPs (t_{exit}) following varying incubation times with partial set of NTPs ($t_{entrance}$). The results (blue) indirectly report on the time it takes to reach the value of the hybridized fraction characteristic for $RP_{ITC\leq 7}$ when starting from $RP_{ITC=2}$ (~7 min). Gray vertical line highlights the hybridized fraction value at $t_{entrance}$ = 40 min, which is the time used throughout this work for exit kinetics. Gray dashed horizontal lines highlight the initial and final levels of the kinetics, which are the same as those in *A*.

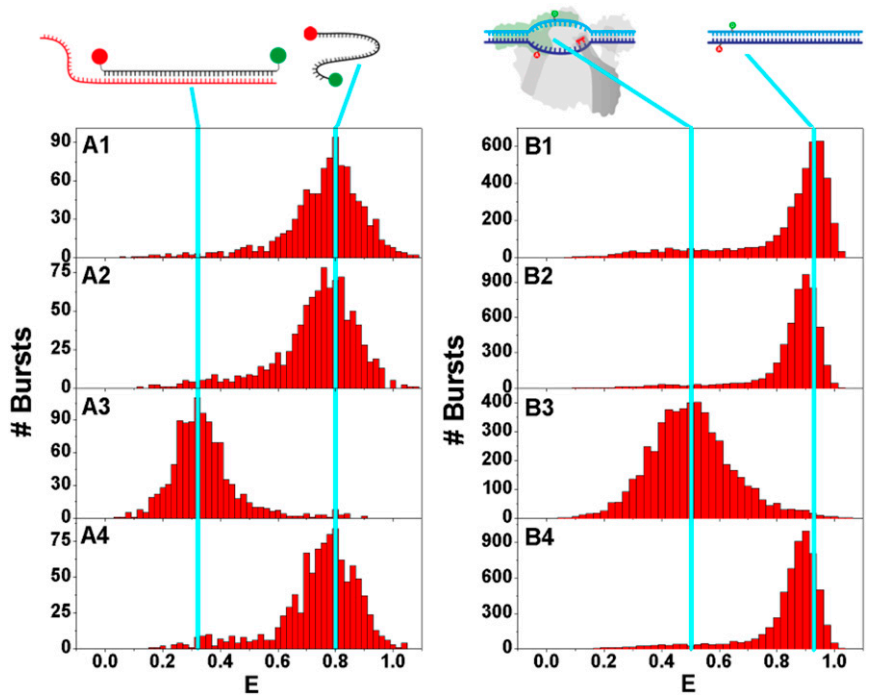

Fig. S5. The effectiveness of GndHCl as a transcription reaction quencher. (*A*) Quantification of runoff transcript production by FRET probe hybridization. The higher FRET peak represents probe only. The lower FRET peak represents probe hybridized to synthesized RNA transcripts. *A1* (probe only) and *A2* ($RP_{ITC=2}$ + probe without NTP) serve as controls. *A3* shows runoff transcript production (GndHCl added only after the reaction is completed). *A4* shows that if GndHCl is added to the reaction mix before the addition of NTPs, the reaction is inhibited. (*B*) Quantification of transcription bubble opening by smFRET. The higher FRET peak represents the free (doubly labeled) promoter DNA. The lower FRET peak represents the promoter DNA with an open bubble ($RP_{ITC=2}$). *B1* (promoter only) and *B2* (promoter + GndHCl) serve as controls. *B3* shows $RP_{ITC=2}$ (promoter + RNAP + A_pA). *B4* shows that if GndHCl is added to $RP_{ITC=2}$, the bubble closes up due to complex dissociation.

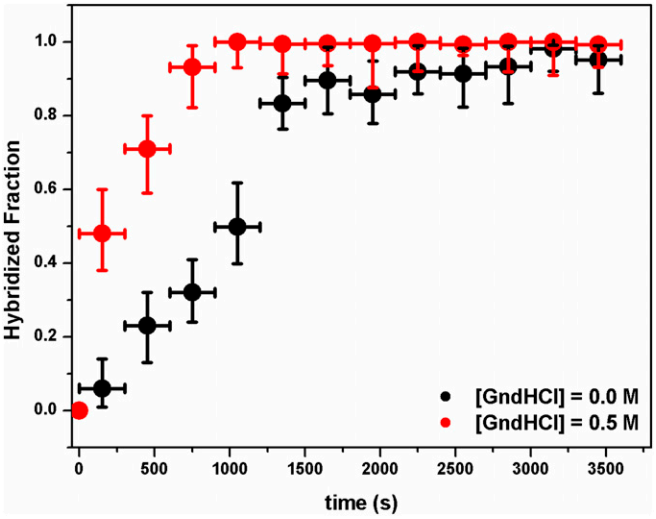

Fig. S6. GndHCl enhances and accelerates ssDNA probe hybridization to RNA transcripts. Shown are real-time hybridization kinetics of 20-dT ssDNA FRET probe to 20A RNA target. A total of 100 pM of probe is added to 100 pM of target at t = 0. smFRET histograms are accumulated at 5-min intervals (*x*-axis errors). Hybridization fraction is extracted from the ratio of the low-FRET subpopulation to the sum of low-FRET and high-FRET subpopulations. The addition of 0.5 M GndHCl to the hybridization mix accelerates the hybridization reaction (red) compared with 0.0 M GndHCl (black) and enhances the hybridization efficiency (red data points above black points at long times).

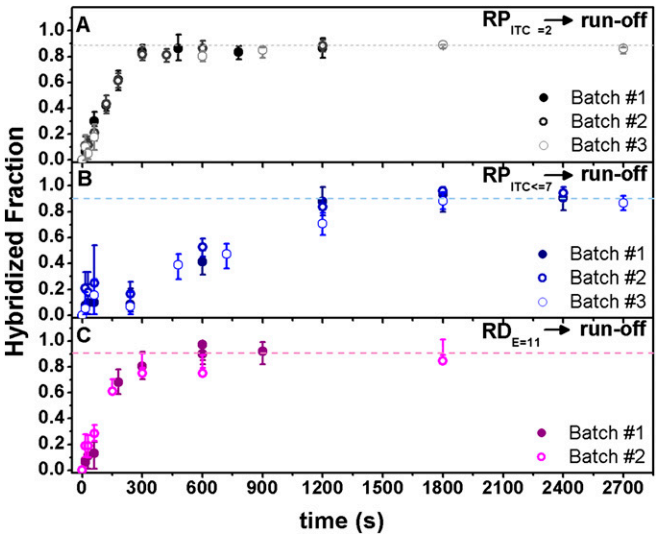

Fig. S7. Reproducibility of the quenched-kinetics assay. Shown are three representative examples of normalized and nonaveraged kinetic data and their measurement repeats using the lacCONS promoter. All batches represent independent experiments performed on different days starting from stock solutions. Error bars for each repeat are derived from the fitting errors of the double-Gaussian global fits of the FRET histograms (as in Fig. 1*C*; with 95% confidence intervals). (*A*) Three experimental repeats of runoff kinetics from $RP_{ITC=2}$. (*B*) Three experimental repeats of runoff kinetics from $RP_{ITC\leq7}$. (*C*) Two experimental repeats of runoff kinetics from $RD_{E=11}$.

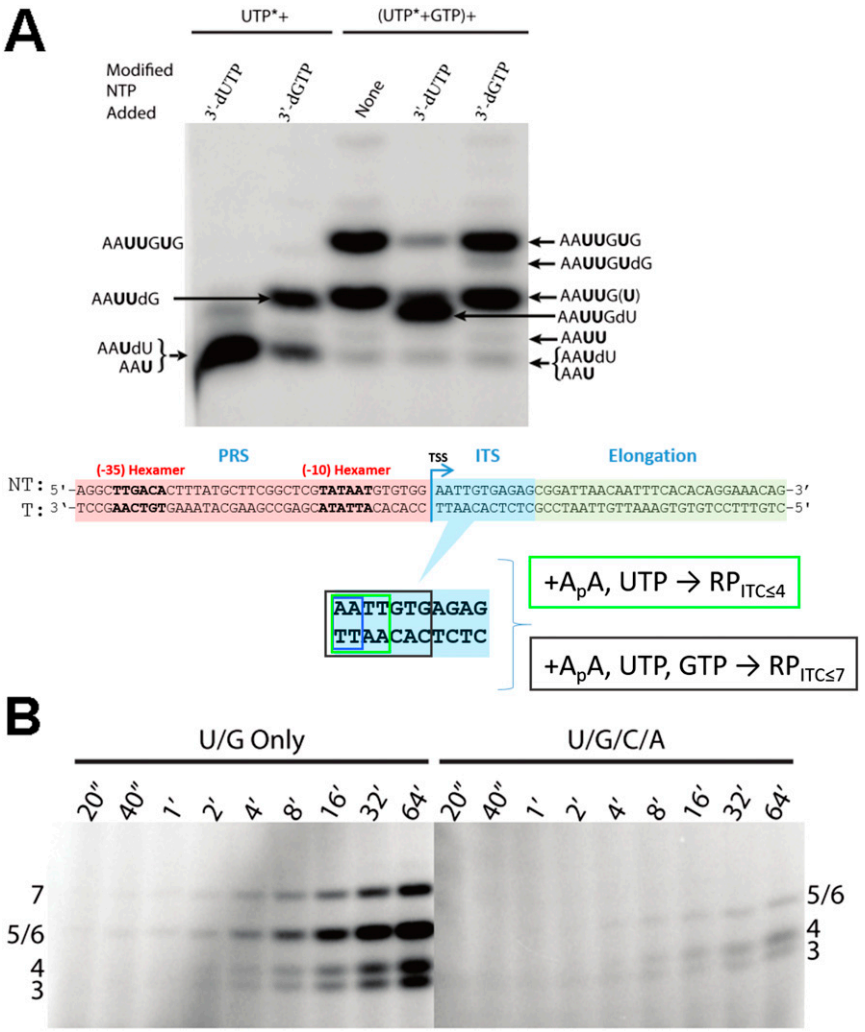

Fig. S8. (*A*) Assignment of abortive products using NTP derivatives. *A, Top* shows different stalled states with the addition of 3′-deoxy nucleotides (3′-dNTPs). The 3′-dNTPs terminate the transcript upon incorporation and also migrate slightly faster, creating a doublet at bands ending with that particular nucleotide. Therefore, the doublet in lane 5 (from the left) shows that the highest band ends in G, suggesting the highest band is indeed the 7-base product (AA**UUGUG**) that would arise from adding only UTP and GTP. Likewise, in lane 4, the top of the doublet in the middle must end in U, revealing that this band is the 6-base product (AA**UUGU**). In addition, in lane 2, the highest band is expected to correspond to the longest transcript terminated at the first G in the sequence (after supplementing the reaction only with UTP), suggesting the highest band is the 5-base product terminated by dGTP (AA**UU**dG). In this context, we conclude that the middle bands in lanes 3–5 are a combination of the 5-base (AA**UUG**) and 6-base products. It is not surprising that these abortive products migrate relatively close together because a single addition of U adds a relatively small amount of mass compared with the addition of a single G. In lane 2, in addition, the lowest two bands are the 3-base and 4-base products (AA**U** and AA**UU**) expected to be produced upon adding only UTP. (*B*) Lack of NTP starvation allows identification of the production of abortive transcripts up to 6 nt. In NTP-starved $RP_{ITC\leq7}$, abortive products are produced up to a size of 7 nt (*Left* gel). However, in the presence of all NTPs, the 7-base abortive product is not produced to an identifiable level (*Right* gel). The 3-base and 4-base products appear in *B* much darker than they appear in *A* because the ethanol precipitation step (used previously in *A*) was skipped, retaining the smaller products.

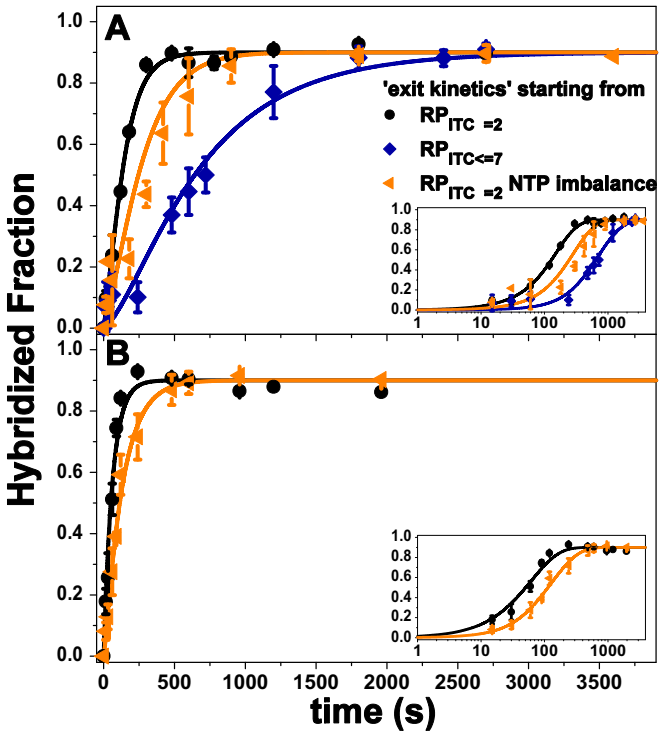

Fig. S9. (*A* and *B*) Transcription runoff kinetics under conditions of NTP starvation/imbalance in lacCONS (*A*) and T5N25 (*B*) promoters. Shown are RNA runoff production kinetic traces (when rescued with all four NTPs) after incubation with equimolar NTP concentrations (100 μM; black), NTP concentration imbalance (UTP and GTP at 100 μM and ATP and CTP at 2 μM in lacCONS promoter; ATP and UTP at 100 μM and CTP and GTP at 2 μM in T5N25 promoter; orange), and full NTP starvation (in lacCONS, $RP_{ITC\leq 7}$ with first incubation with no ATP and CTP and then adding all four NTPs at 100 μM; blue). The data are represented as points and solid lines represent best-fit results to the model described in *Methods*. The best-fit values of the model parameters are shown in Table S1.

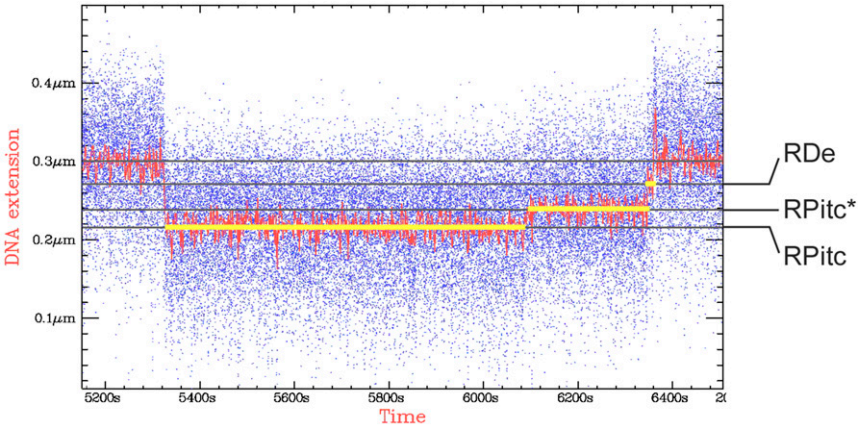

Fig. S10. lacCONS promoter. Magnetic bead extension shows signature of the paused–backtracked state in the absence of initiating dinucleotide, A_pA. Example of a DNA-extension trajectory obtained in the absence of GreA displays the initially transcribing complex, RP_{ITC}, the backtracked initially transcribing complex, RP_{ITC}*, and ultimately promoter escape and formation of a fully competent elongation complex, RD_E. Gray lines and yellow lines are guides to the eye underscoring the above states and their durations. Experiments were carried out under conditions essentially identical to those in Fig. 4, but without the use of an initiating dinucleotide.

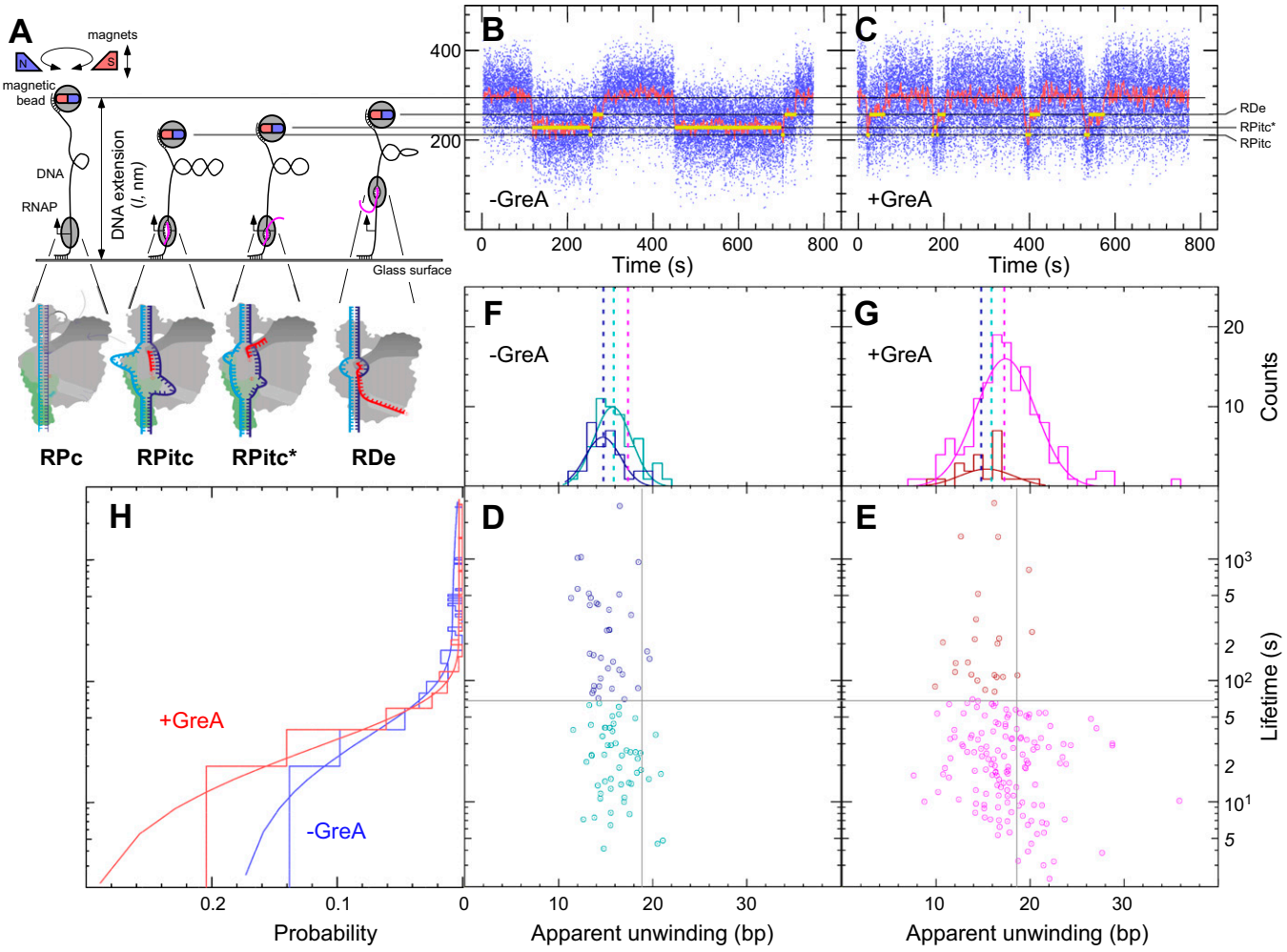

Fig. S11. T5N25 promoter. Backtracking in initiation is correlated with pausing in the presence of all NTPs and the initiating dinucleotide, A_pU. (*A*) Schematics of the magnetic tweezer transcription assay. (*B* and *C*) Representative DNA extension trajectories are shown for experiments in the absence (*B*) or presence (*C*) of 1 μM GreA. Experiments were carried out under conditions identical to those in Fig. 4, but with the use of the initiating dinucleotide, A_pU, relevant to the T5N25 promoter sequence. One can observe unwinding levels (gray lines) associated with the different bubble sizes imposed by the different transcription states. Yellow lines highlight typical lifetimes in RP_{ITC} and RP_{ITC} states. (*D–H*) The unwinding levels and lifetimes of individual initiation events (i.e., averaging over all RP_{ITC} and RP_{ITC}* states seen from initiation to promoter escape) are summarized into unwinding–lifetime scatter plots in which GreA was either absent (*D*, n = 87) or present (*E*, n = 164) and their 1D projections are shown in *F–H*. The scatter plots (*D* and *E*) are divided into quadrants to highlight the change in the results upon the addition of GreA on the basis of lifetime and unwinding levels (*Methods*, , *Illustrations*). Lifetime data in the absence or presence of GreA were first fitted to single or double exponentials based on goodness-of-fit. Then, the 2D data were temporally separated into events shorter than (cyan, absence of GreA; magenta, presence of GreA) or longer than (dark blue, absence of GreA; dark red, presence of GreA) the fast timescale for promoter escape (~300 s) plus 1 SD. Similarly, the 2D data were spatially separated into events with apparent unwinding amplitude smaller or larger than the mean unwinding observed during short-duration escape events plus 1 SD. Apparent unwinding data associated with short- or long-escape timescales were then fitted to single- or double-Gaussian distributions based on goodness-of-fit and according to the color code described above. Dotted vertical lines are visual guides to the maximum of the respective Gaussian distributions. In the absence of GreA, the fast timescale for productive escape from this promoter was 32 ± 3 s (SEM) and was correlated to apparent DNA unwinding of 15.7 ± 0.3 bp SEM (with SD 2 ± 0.3 bp SEM). The slow timescale was on the order of thousands of seconds and correlated to smaller apparent unwinding (14.7 ± 0.5 bp SEM, with SD 1.9 ± 0.5 bp SEM). In the presence of GreA we instead observed essentially a uniform population capable of rapid promoter escape (32 ± 3 s) correlated to larger apparent DNA unwinding (17.4 ± 0.3 bp SEM, with SD 3.2 ± 0.3 bp SEM).

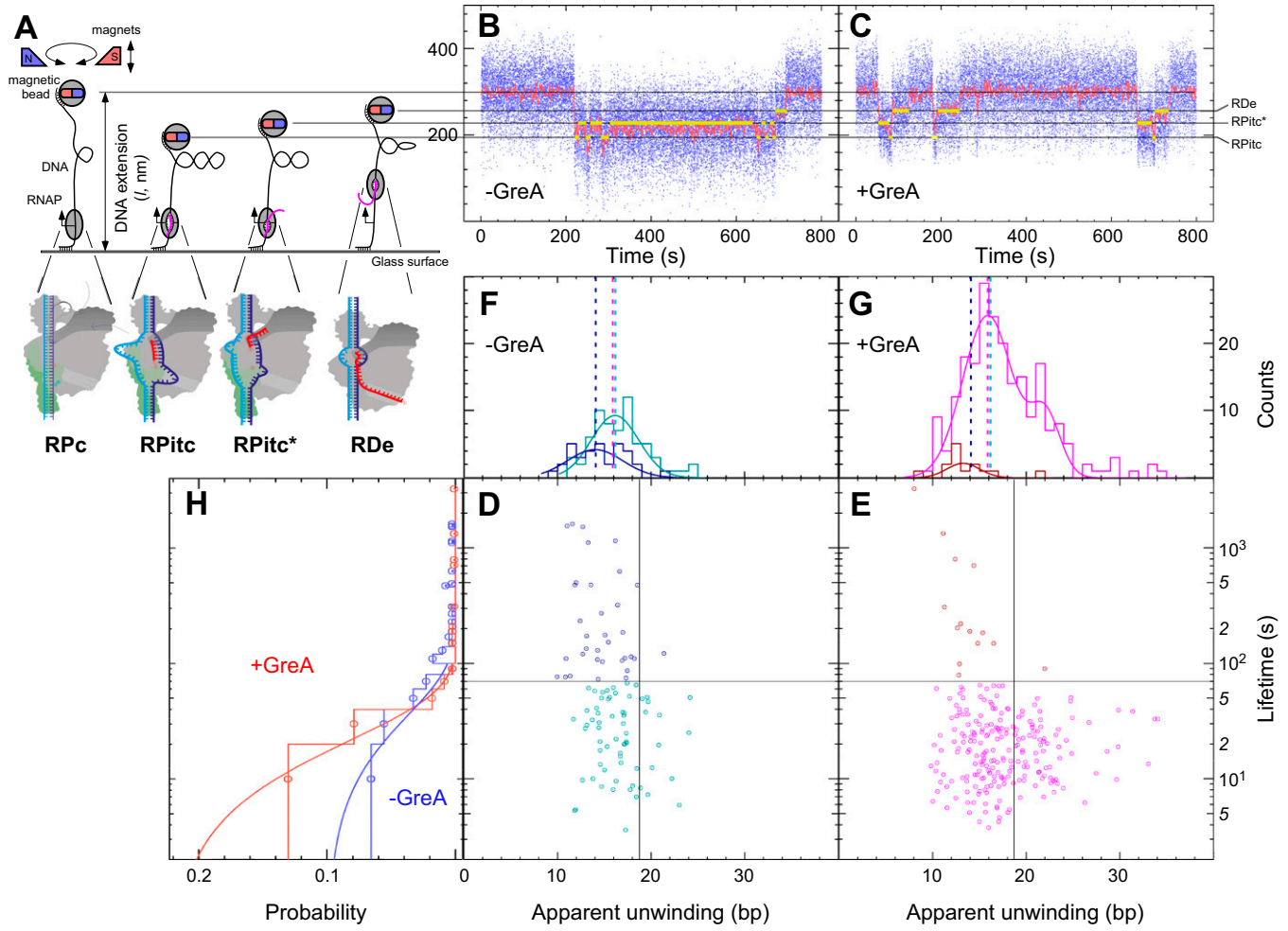

Fig. S12. T5N25 promoter. Backtracking in initiation is correlated with pausing in the presence of all NTPs with no initiating dinucleotide, A_pU. (*A*) Schematics of the magnetic tweezer transcription assay. (*B* and *C*) Representative DNA-extension trajectories are shown for experiments in the absence (*B*) or presence (*C*) of 1 μM GreA. Experiments were carried out under conditions identical to those in Fig. 4, but without the use of initiating dinucleotide, A_pU. One can observe unwinding levels (gray lines) associated with the different bubble sizes imposed by the different transcription states. Yellow lines highlight typical lifetimes in RP_{ITC} and RP_{ITC}* states. (*D–H*) The unwinding levels and lifetimes of individual initiation events (i.e., averaging over all RP_{ITC} and RP_{ITC}* states seen from initiation to promoter escape) are summarized into unwinding–lifetime scatter plots in which GreA was either absent (*D*, n = 99) or present (*E*, n = 234) and their 1D projections are shown in *F–H*. The scatter plots (*D* and *E*) are divided into quadrants to highlight the change in the results upon the addition of GreA on the basis of lifetime and unwinding levels (*Methods*, , *Illustrations*). Lifetime data in the absence or presence of GreA were first fitted to single or double exponentials based on goodness-of-fit. Then, the 2D data were temporally separated into events shorter than (cyan, absence of GreA; magenta, presence of GreA) or longer than (dark blue, absence of GreA; dark red, presence of GreA) the fast timescale for promoter escape (~300 s) plus 1 SD. Similarly, the 2D data were spatially separated into events with apparent unwinding amplitude smaller or larger than the mean unwinding observed during short-duration escape events plus 1 SD. Apparent unwinding data associated with short- or long-escape timescales were then fitted to single- or double-Gaussian distributions based on goodness-of-fit and according to the color code described above. Dotted vertical lines are visual guides to the maximum of the respective Gaussian distributions. In the absence of GreA, the fast timescale for productive escape from this promoter was 36 ± 6 s (SEM) and was correlated to apparent DNA unwinding of 16.1 ± 0.4 bp SEM (with SD 2.5 ± 0.4 bp SEM). The slow timescale was on the order of thousands of seconds and correlated to smaller apparent unwinding (14 ± 0.8 bp SEM, with SD 2.9 ± 0.7 bp SEM). In the presence of GreA we instead observed uniformly rapid promoter escape (with mean lifetime 22 ± 2 s) correlated to larger apparent DNA unwinding displaying multimodal behavior.

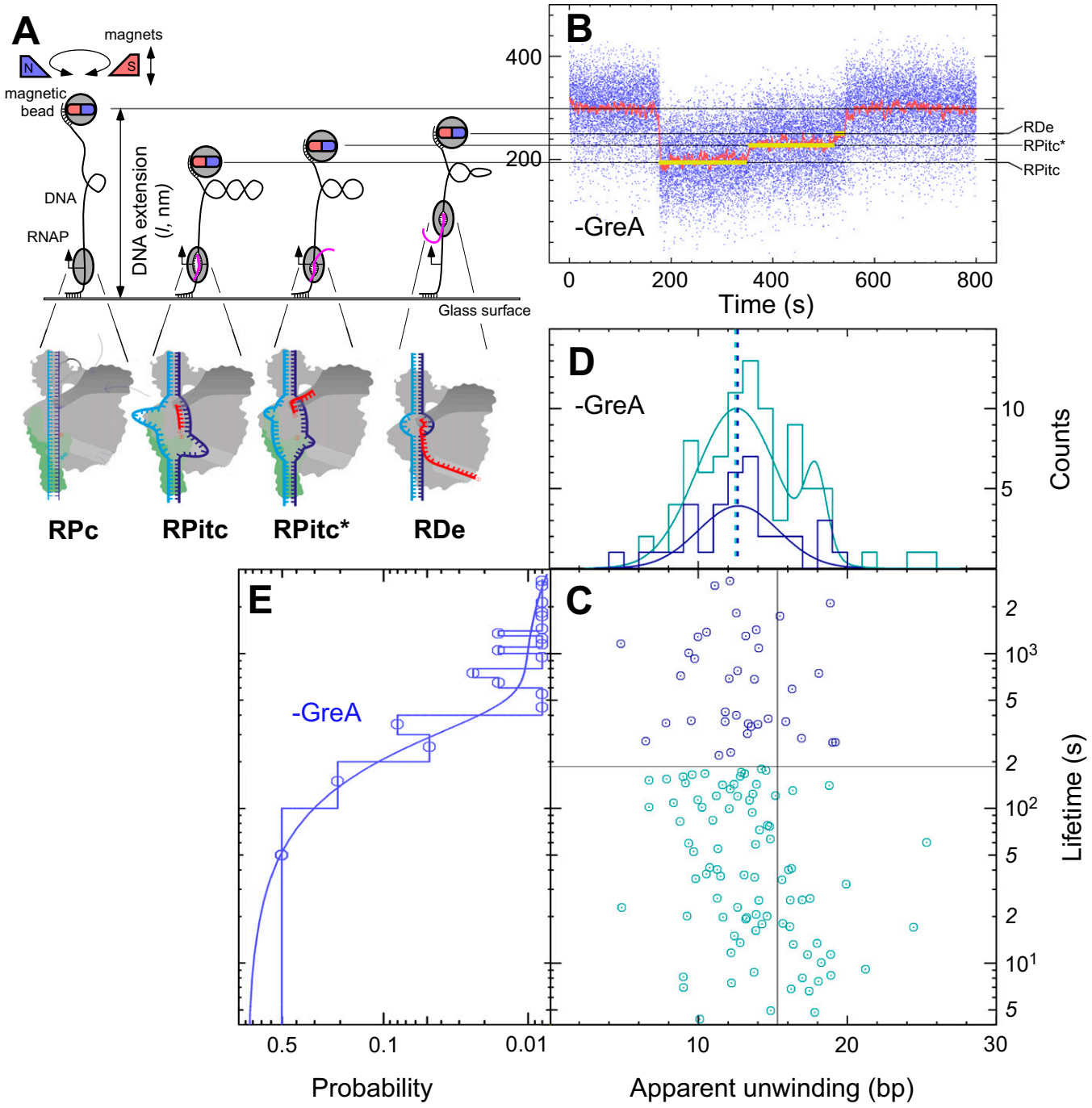

Fig. S13. lacCONS promoter. Backtracking in initiation is correlated with pausing in the presence of all NTPs at 1 mM each. (*A*) Schematics of the magnetic tweezer transcription assay. (*B*) Representative DNA-extension trajectory is shown for experiments in the absence of GreA showing the long-lived, backtracked state RP_{ITC}*. Experiments were carried out under conditions identical to those in Fig. 4, but without the use of initiating dinucleotide, A_pA. One can observe unwinding levels (gray lines) associated with the different bubble sizes imposed by the different transcription states. Yellow lines highlight typical lifetimes in RP_{ITC} and RP_{ITC}* states. (*C*–*E*) The unwinding levels and lifetimes of individual initiation events (i.e., averaging over all RP_{ITC} and RP_{ITC}* states seen from initiation to promoter escape) are summarized into unwinding–lifetime scatter plots when GreA was absent (*C*, n = 125) and their 1D projections are shown in *D* and *E*. The scatter plot (*C*) is divided into quadrants to highlight the change in the results upon the addition of GreA on the basis of lifetime and unwinding levels (*Methods*, *Illustrations*). Lifetime data in the absence or presence of GreA were first fitted to single or double exponentials based on goodness-of-fit. Then, the 2D data were temporally separated into events shorter than (cyan, absence of GreA; magenta, presence of GreA) or longer than (dark blue, absence of GreA; dark red, presence of GreA) the fast timescale for promoter escape (~300 s) plus 1 SD. Similarly, the 2D data were spatially separated into events with apparent unwinding amplitude smaller or larger than the mean unwinding observed during short-duration escape events plus 1 SD. Apparent unwinding data associated with short- or long-escape timescales were then fitted to single- or double-Gaussian distributions based on goodness-of-fit and according to the color code described above. Dotted vertical lines are visual guides to the maximum of the respective Gaussian distributions. We again observed a fast timescale for promoter escape (reduced to 91 ± 15 s in these elevated NTP conditions) and a slow timescale for promoter escape in the thousands of seconds. The data were not sufficient to clearly distinguish a difference between apparent unwinding amplitudes for the fast and slow timescales.

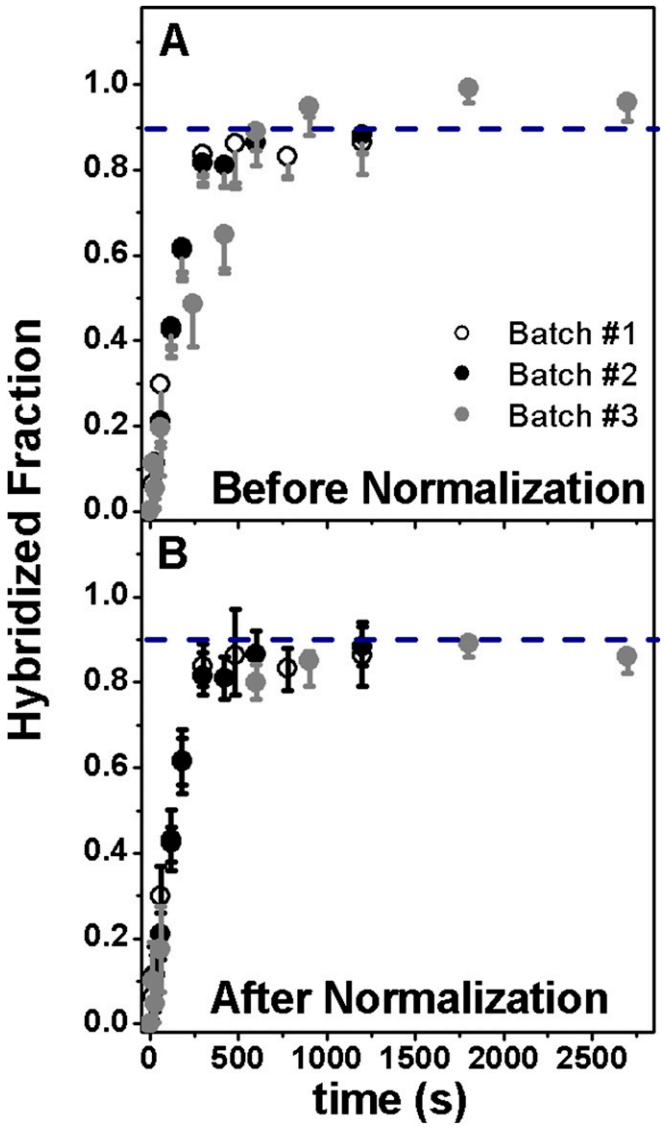

Fig. S14. Rescaling of kinetics to a common steady-state value. Shown are three experimental repeats of runoff kinetics from $RP_{ITC=2}$, using the lacCONS promoter, before (*A*) and after (*B*) rescaling the repeated experimental results to a common value of 0.9. Note how before rescaling, the raw experimental results all reach a steady-state plateau close to 0.9. However, to retrieve the average and SD of kinetic experiments, the experimental repeats have to reach exactly the same steady-state plateau and not be only close to it.

Table S1. Best global fit values of transition rates and subpopulation fractions using a simplified abortive initiation model

Promoter	GreA	Exit out of	$k_{on\rightarrow off}$, 10^{-3} s^{-1}	$k_{off\rightarrow on}$, 10^{-3} s^{-1}	$k_{init\rightarrow elon}$*, 10^{-3} s^{-1}	On-pathway initial population	Fig./panel/color
lacCONS	–	$RP_{ITC=2}$	—	—	6 ± 1†	1.00 (const.)‡	Fig. 1*D*/black; Fig. 2/black; Fig. 3*A*/black; Fig. S9*A*/black;
lacCONS	–	$RP_{ITC\leq4}$	(0–1)§	3.7 ± 0.6		0.20 ± 0.06	Fig. 2/red
lacCONS	–	$RP_{ITC\leq6}$	(0–1)	3.4 ± 0.5		0.15 ± 0.05	Fig. 2/green
lacCONS	–	$RP_{ITC\leq7}$	(0–1)	1.7 ± 0.3		0.07 ± 0.03	Fig. 2/blue; Fig. 3*A*/blue; Fig. S9*A*/blue;
lacCONS	–	$RD_{E=11}$	—	—	13 ± 2	1.00 (const.)	Fig. 2/magenta
lacCONS	+	$RP_{ITC=2}$	—	—	4 ± 1	1.00 (const.)	Fig. 3*B*/black
lacCONS	+	$RP_{ITC\leq7}$	(0–1)	4.1 ± 0.9		0.51 ± 0.15	Fig. 3*B*/blue
T5N25	–	$RP_{ITC=2}$ all NTPs equal¶	—	—	16 ± 3	1.00 (const.)	Fig. S9*B*/black
T5N25	–	$RP_{ITC=2}$ NTP imbalance#	18 ± 5	26 ± 8		0.23 ± 0.07	Fig. S9*B*/orange
lacCONS	–	$RP_{ITC=2}$ NTP imbalance‖	(0–1)	6.5 ± 0.8	6 ± 1	0.28 ± 0.11	Fig. S9*B*/orange

*Initiation → elongation.
†This parameter is globally shared in the model as one can assume the initiation → elongation rate constant does not change for a given promoter in a given condition.
‡The initial conditions are set to constant values (const.) in the case where by design there is no population of the off-pathway state at t = 0, such as when starting from $RP_{ITC=2}$.
§The best-fit result was converging to a value of 0. The statistical upper bound value was the one reported in parentheses.
¶All NTPs at 100 μM.
#ATP and UTP at 100 μM and GTP and CTP at 2 μM.
‖UTP and GTP at 100 μM and ATP and CTP at 2 μM.